FINAL TECHNICAL REPORT

U.S. Geological Survey
National Earthquake Hazards Reduction Program

Award Number G18AP00093

Deformation rates, detailed mapping, and seismic hazard of the Black Butte–San Joaquin fold and thrust belt adjacent to the Sacramento–San Joaquin Delta: Collaborative Research with Oregon State University and the U.S. Geological Survey.

by

Yann Gavillot[1,2] and Andrew Meigs[1]

[1]College of Earth, Ocean, and Atmospheric Sciences**,** Oregon State University
104 Admin Building, Corvallis, OR 97331

[2]now at Montana Bureau of Mines and Geology, Montana Technological University
1300 W. Park Street, Butte, MT 59701
Email: ygavillot@mtech.edu; Phone: (406) 496-4890

Term of Award:
September 1, 2018 – December 31, 2020

Research supported by the U.S. Geological Survey (USGS), Department of the Interior, under USGS award number G18AP00093. The views and conclusions contained in this document are those of the authors and should not be interpreted as representing the opinions or policies of the U.S. Geological Survey. Mention of trade names or commercial products does not constitute their endorsement by the U.S. Geological Survey.

ABSTRACT

The eastern margin of the Diablo Range near the Sacramento and San Joaquin Delta in northern California is characterized by west-dipping reverse or thrust faults associated with the Great Valley thrust system (GVT). Though subsidiary to the San Andreas fault system, seismic hazards from GVT faults are not well constrained, and even moderate shaking could profoundly affect the vulnerable infrastructure and ecology of the Delta region. At the latitude of Tracy and Livermore, the GVT is represented by the Black Butte and San Joaquin faults, a system of overlapping faults that extends for more than 85 km along the Diablo Range mountain front. We conducted new detailed geologic and geomorphic mapping, structural analyses, high resolution topographic data analyses, and Quaternary dating to provide new constraints of subsurface fault geometry, slip rates, and earthquake potential for the Black Butte–San Joaquin fault system at the Corral Hollow Creek and Lone Tree Creek study sites.

New age data from syntectonic Plio-Pleistocene alluvial strata reveal sustained and coeval deformation on the Black Butte and San Joaquin faults since 600–800 ka to at least 211–100 ka. Folded and faulted terraces constrain fault activity on the Black Butte–San Joaquin fault system since ~105 ka, including the youngest fold scarp which is no older than ~13 ka. Bedrock mapping and fault exposures indicate the Black Butte fault is an emergent 38–42°SW-dipping transpressional thrust that juxtaposes folded Cretaceous–Miocene bedrock over Plio-Pleistocene units overlain by fluvial terraces. Field observations indicate fault displacement on the BBF reflects a combination of thrust and strike-slip deformation. Vertical separation of a 105.0 ± 18.1 ka terrace offset across the Black Butte fault yields a minimum long-term fault slip rate of 1.3–2.0 mm/yr. The San Joaquin fault is a 30–42°SW dipping blind thrust that deforms Plio-Pleistocene alluvial strata and fluvial terraces along the range front. Incision and fault-related uplift of multiple dated strath terraces yield long-term average fault slip rate of 0.9–1.7 mm/yr since ~100 ka on the San Joaquin fault. Combined rates for the Black Butte-San Joaquin fault system yield a total fault slip rate budget of 2.2–3.7 mm/yr and shortening rate of 1.7–3.0 mm/yr, which is consistent with a comparison of geodetic derived shortening rates (1.9–3.5 mm/yr) for the eastern Diablo Range. Structural relations suggest that the faults are east-verging contractional splays that link at depth. Scaling and empirical relations suggest potential earthquake magnitudes ranging from Mw 6.2 to Mw 7.3 for reverse fault rupture earthquakes. Associated seismic hazard from the Black Butte–San Joaquin fault is potentially equal to or greater than Vacaville–Winters earthquake sequence (1892 Mw 6.4–6.2) or Coalinga earthquake (1985 Mw 6.3). The Black Butte–San Joaquin fault system thus poses a significant risk to the Sacramento-San Joaquin Delta region, the critical water resource infrastructure, and the nearby San Francisco East Bay population center.

1. INTRODUCTION

The Sacramento–San Joaquin Delta encompasses vital agricultural, ecological, and water resources to the state of California, and is home to over half million people. Earthquake ground shaking damage could profoundly affect and intensify the vulnerability of the Delta to flooding and subsidence, which can compromise California's critical water delivery infrastructure (levee systems, canals, and pipelines). Seismic sources that could affect the Delta are well recognized from major fault strands associated with the strike-slip San Andreas Fault system further west in the San Francisco Bay Area (e.g., UCERF3; Field et al., 2013). Many faults in the Bay Area are characterized by readily observable geomorphic expressions of faulting, high slip rates, creep, moderate to high seismicity, and episodic historical damaging surface-rupturing earthquakes (1868 Mw 6.8 Hayward; 1906 Mw 7.8 San Francisco; 1989 Mw 6.9 Loma Prieta). On the other

hand, seismic source characterizations for subsidiary faults to the San Andreas Fault system near the Delta are either not included or not well constrained in existing hazards analyses. These faults proximal to the Delta could pose larger seismic hazards than primary segments of the San Andreas Fault system in generating potential strong earthquake ground shaking.

The Black Butte and San Joaquin faults represent some of the least understood fault segments associated with the Great Valley thrust system (UCERF3, Field et al., 2013), which poses a substantial shaking hazard to the nearby Sacramento–San Joaquin Delta. The Black Butte–San Joaquin fault system is characterized by overlapping poorly-defined transpressional faults and folds and blind fault segments, which deform surficial sediments between the eastern Diablo Range piedmont and California Central Valley. Both faults are listed individually in the USGS Q-fault database and previously identified in their map extent with evidence of Quaternary fault activity (Diblee, 1981a; 1981b; Noller et al., 1993; Sowers et al., 1993; Sowers et al., 1998). A lack of detailed field relations of surface deformation and adequate age data preclude understanding of fault-fold history, subsurface fault geometry, slip rates, and seismic source characterization. A fault slip rate estimate of 0.08–0.54 mm/yr is available from a fold scarp site that affects Pleistocene terraces across the blind San Joaquin fault (Sowers et al., 2000). Absolute age data and slip rate estimates for the Black Butte fault do not exist, despite the fact that the fault clearly shows evidence of late Quaternary fault activity. Given the proximity of these two faults, evidence of deformed geomorphic surfaces, faults exposures, and appropriate deposits for Quaternary dating (terrestrial cosmogenic nuclide ^{10}Be depth profiles, luminescence dating) provided the motivation to investigate the Black Butte and San Joaquin faults for seismic source characterization.

In this final technical report, we present new detailed mapping, high resolution topographic data with measurements of deformation (Lidar, UAV drone photogrammetry, NED DEM), and age data (IRSL and TCN ^{10}Be depth profiles) to define structural fault geometry and Pleistocene–Holocene fault slip rates of the Black Butte–San Joaquin fault system. Our study sites are located near the drainages of Corral Hollow Creek and Lone Tree Creek, characterized with well-preserved deformed alluvial surfaces and multiple fault scarps (Figs. 1 and 2a, 2b, 2c). Improved knowledge of the fault geometry and slip rates provide new constraints on the characterization of the late Quaternary fault history and earthquake potential. Our study provides new data that constrain the total fault slip budget, shortening, and partitioning across this fault system. These new data can be compared to other faults splays associated with the Great Valley thrust in the Delta region (West Tracy Fault; Unruh and Hitchcock, 2015), and to geodetic data of shortening across the eastern Diablo Range (1.9–3.5 mm/yr; d'Alessio et al., 2005; Prescott et al., 2001). Our results support ongoing efforts to update geological parameters and improve regional deformation models used in seismic hazard assessments using the Northern California fault set in Community Fault Model, UCERF3, and Delta Risk Management (DRMS) for the Sacramento and San Joaquin Delta and its infrastructure. Moreover, this study improves our understanding on the regional tectonics and uplift history the Coast and Diablo Ranges.

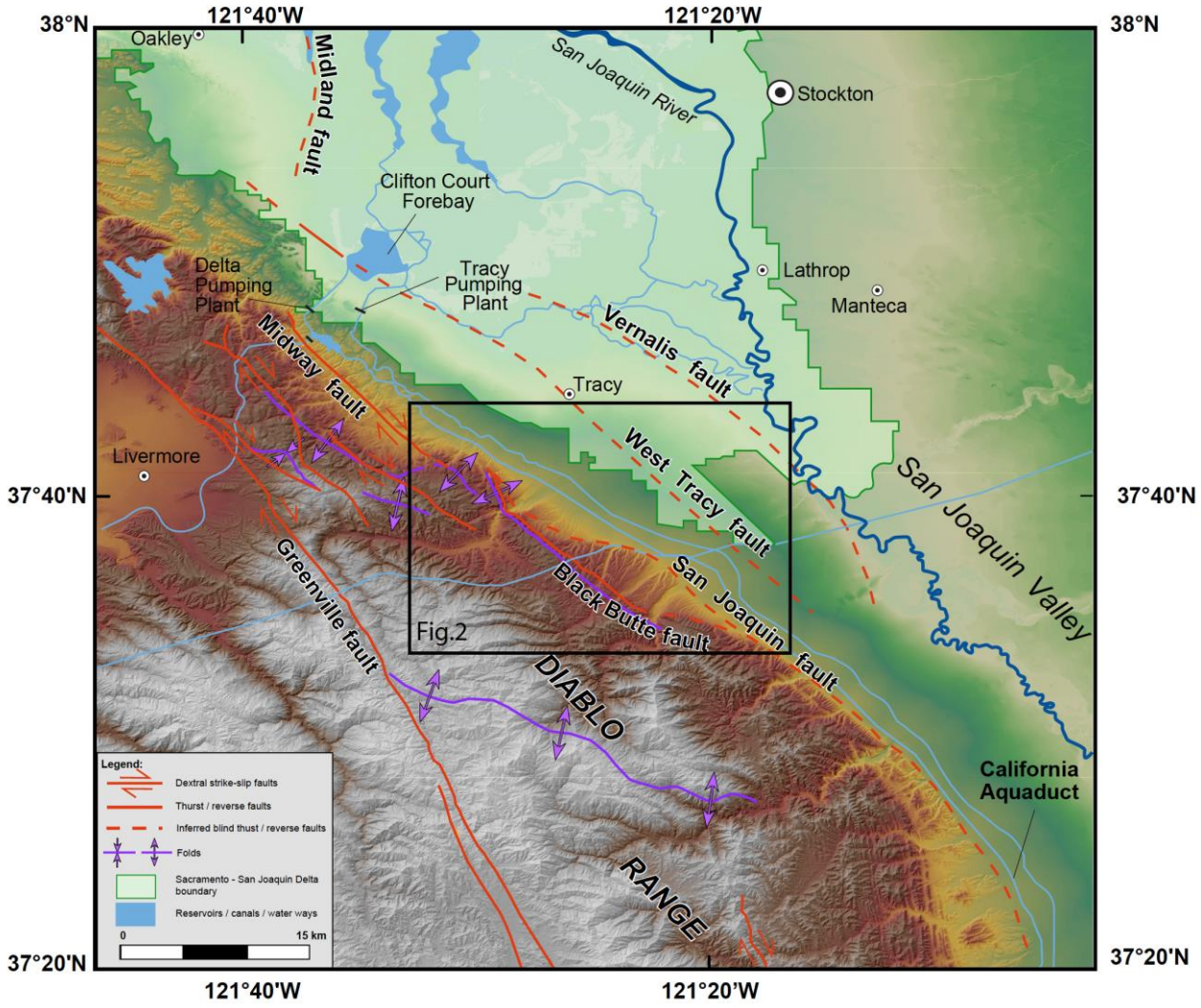

Figure 1. Fault and location map for the southern Sacramento-San Joaquin Delta and Diablo Range with study sites shown in Figure 2. Mapped faults and folds are from the USGS Q Faults database, supplemented from Sowers et al. (2000), Unruh and Krug (2007), Unruh and Hitchcock, (2015), and this study.

GEOLOGIC SETTING

Discontinuous segments of fault-related *en echelon* folds and west-dipping thrusts mark the physiographic boundary between the eastern Diablo Range and the western margin of the San Joaquin Valley (Fig. 1). The faults are collectively referred to as the Great Valley thrust system (UCERF3, Field et al., 2013; see Appendix A, Dawson, 2013), previously known as the Coast Range–Sierran Block tectonic boundary zone (e.g., Wong et al., 1988). Most of these thrust segments are interpreted to be blind, as evidenced by the uplift, tilting, and folding of Quaternary sediments (Unruh et al., 1992; Sowers et al., 1993a; Noller et al., 1993; Sowers et al., 2000; Anderson and Piety, 2001, Unruh and Krug, 2007), as well as limited seismic and well log data (Krug et al., 1992; Sterling, 1992; Unruh and Hitchcock, 2015).

In the southern Sacramento–San Joaquin Delta region, the Great Valley thrust system comprises multiple faults splays and fault-related folds, which include the Black Butte, San

Joaquin, Midway, West Tracy, and Vernalis faults (Fig. 1; Jennings et al., 1994; Unruh and Krug, 2007; Jennings and Bryant, 2010). The Black Butte fault, Midway fault, and locally West Tracy fault have documented near-surface faulting evidenced by offset Quaternary surficial deposits and potential fault scarps within the eastern Diablo Range foothills (Diblee, 1981; 1981b; Noller et al., 1993; Unruh and Sawyer, 1995; Unruh and Hitchcock, 2015). The San Joaquin (Orestimba), West Tracy, and Vernalis faults are blind. Fold scarps in Pleistocene alluvial deposits have been interpreted as fault-related deformation above the blind San Joaquin fault along the mountain front (Sowers et al., 1998; 2000). The West Tracy fault and Vernalis fault located further into the San Joaquin Valley, are interpreted as range parallel west-dipping faults based on limited seismic data (Krug et al., 1992; Sterling, 1992; Unruh and Hitchcock, 2015). Kinematic models argue that active tectonic wedging beneath the Eastern California Coast Ranges and Diablo Range links these faults to deeper structures and/or detachments (Wentworth et al. 1984; Wakabayashi and Unruh, 1995; Jachens et al., 1995; Guzofski et al., 2007). Alternatively, other models argue that segments of the Great Valley thrusts represent isolated and local transpressional faults (e.g., Unruh and Krug, 2007), or reactivated Cretaceous–early Tertiary normal faults with post-Miocene reverse or oblique reverse sense of motion (Unruh and Hitchcock, 2015).

Earthquake frequency, Quaternary fault activity and strain rates for the southern Delta region are either poorly constrained or unknown. The only known historic earthquake sourced within the Delta occurred during the 1892 Mw 6.4–6.2 Vacaville–Winters earthquake sequence, interpreted to be sourced on a blind thrust ramp with no surface rupture, similar to the strain release associated with the 1985 Mw 6.3 Coalinga earthquake (O'Connel et al., 2001; Guzofski et al., 2007). Geological slip rates based on in-situ absolute age data are limited to the San Joaquin and West Tracy faults. A fold scarp on the San Joaquin fault at Lone Tree Creek (Fig. 2c), suggests fault slip rates of 0.08–0.54 mm/yr for the 69–24 ka time period assuming a 30–60° fault dip based on U-series and ^{14}C dating of carbonate weathering rinds (Sowers et al., 2000). On the West Tracy fault, work by Unruh and Hitchcock (2015) near the Clifton Court Forebay (Fig. 1), provides vertical separation rates of 0.23–0.34 mm/yr from Neogene to Holocene timescales based on structural relief of Miocene sediments (reprocessed seismic reflection data) and offset marshland peat deposits (geotechnical borings). Geodetic data suggest both strike-slip and convergence motions characterize the western edge of the San Joaquin Valley with shortening rates of 1.9–3.5 mm/yr and dextral strike-slip rates of 4.4–6.4 mm/yr (Prescott et al., 2001; d'Alessio et al., 2005). Comparison of available geologic shortening and fault slip rates (<1 mm/yr) for the faults segments associated with the Great Valley thrust system highlights a contrast to the geodetic-derived convergence rates (1.9–3.5 mm/yr).

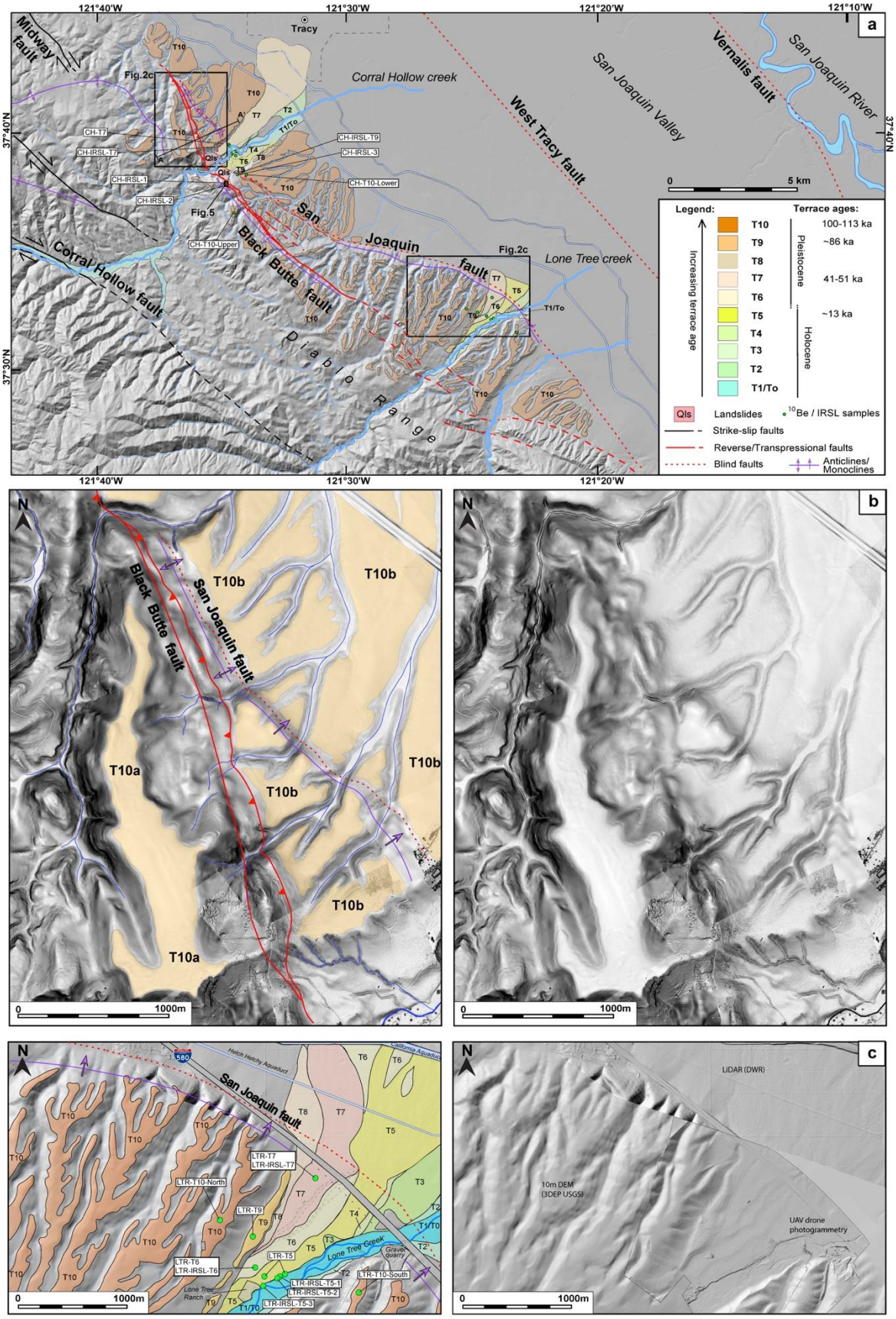
a
121°40'W
121°30'W
121°20'W
121°10'W
37°40'N
37°30'N
Tracy
Midway fault
Corral Hollow creek
West Tracy fault
San Joaquin Valley
Vernalis fault
San Joaquin River
Fig.2c
Fig.5
CH-T7
CH-IRSL-T7
CH-IRSL-1
CH-IRSL-2
CH-IRSL-T9
CH-IRSL-3
CH-T10-Lower
CH-T10-Upper
Qls
San Joaquin fault
Black Butte fault
Corral Hollow fault
Lone Tree creek
Diablo Range
0
5 km
Legend:
Terrace ages:
Increasing terrace age
T10
T9
T8
T7
T6
T5
T4
T3
T2
T1/To
Pleistocene
Holocene
100-113 ka
~86 ka
41-51 ka
~13 ka
Landslides
10Be / IRSL samples
Strike-slip faults
Reverse/Transpressional faults
Blind faults
Anticlines/ Monoclines
b
N
T10b
T10a
0
1000m
c
Hetch Hetchy Aqueduct
California Aqueduct
580
LTR-T7
LTR-IRSL-T7
LTR-T10-North
LTR-T9
LTR-T5
LTR-T6
LTR-IRSL-T6
LTR-IRSL-T5-1
LTR-IRSL-T5-2
LTR-IRSL-T5-3
LTR-T10-South
Lone Tree Creek
Gravel quarry
Lone Tree Ranch
LiDAR (DWR)
10m DEM (3DEP USGS)
UAV drone photogrammetry

Figure 2. a) Quaternary and geomorphic map of the Black Butte–San Joaquin fault system with study sites at Corral Hollow Creek and Lone Tree Creek. Detailed quaternary maps are shown for **b)** North Corral Hollow Creek and **c)** Lone Tree Creek based on Slope Hillshade or Hillshade LiDAR DEM (USGS 3DEP, DWR) and UAV drone photogrammetry. Where neither were available, the base map is a 10m DEM (3DEP USGS) and field mapping was based on Google Earth imagery. Note the close proximity of major water infrastructure (California Aqueduct, Hetch Hetchy Aqueduct) and major transportation corridor. Sample locations for IRSL and TCN ^{10}Be geochronology shown by green circles.

STRUCTURAL MAPPING OF THE BLACK BUTTE-SAN JOAQUIN FAULT SYSTEM

The Black Butte–San Joaquin fault system defines a ~30km-long zone of overlapping faults and folds that trends NW-SE along the eastern foothills of the Diablo Range (Figs. 1 and 2a). This fault system extends to ~85 km a long strike and continues as the San Joaquin fault to the southeast near Patterson. Potential linkage to the Midway fault to the northwest would extend the fault system to ~100 km (Fig. 1). Map relations, cross sections, Plio-Pleistocene alluvial strata, and the surface deformation pattern suggest that the Black Butte and San Joaquin faults are linked and act as structurally and temporally integrated fault system.

The Black Butte–San Joaquin fault system is characterized by two major NW-SE-trending fault segments bounding a zone up to ~5km wide that include additional fault splays (Fig. 2a). The Black Butte fault (BBF) is best exposed in Corral Hollow Creek, as an emergent to shallow transpressional fault that extends ~30 km along the eastern Diablo Range piedmont (Figs. 2a and 2b). The BBF juxtaposes in its hanging wall Cretaceous Great Valley Group marine clastics (Panoche Fm) and overlying Miocene non-marine rocks (Neroly Fm) against deformed Plio-Pleistocene deposits in the footwall (Figs. 3 and 4). In the Corral Hollow Creek, the Panoche Fm dips 30–40°SW near the fault trace. Further west, dips shallow to 15–25°SW associated an anticline fold limb (Figs. 2a and 4). Overlying Miocene bedrock strata are characterized by an angular unconformity with dips 10-15° WSW and preserve a fault-bend fold anticlinal structure (Figs. 3 and 4). South of the Corral Hollow Creek, similar hanging wall anticlinal folds parallel the fault trace (Fig. 2a). Two additional angular unconformities mark the basal contacts with overlying Plio-Pleistocene units and terrace deposits (Figs. 3 and 4). Sequential folding, multiple angular unconformities, and juxtaposition of Cretaceous–Miocene bedrock with Quaternary sediments suggest the of BBF has a protracted long-term fault history characterized by multi-phase thrust related deformation since the Miocene (Fig. 4). Natural fault exposures of local fault splays along BBF reveal a 40° (± 2°) SW-dip and fault zone marked by breccia, mineralization, and a sheared and highly fractured damage zone (Fig. 5). Evidence of strike-slip deformation in outcrops include subvertical faults and shear fractures with oblique slickenlines cross cutting the low angle BBF (Fig. 5). No clear lateral offset markers were recognized in the field, which may suggest any component of dextral strike-slip deformation is primarily accommodated on other structures (i.e., Midway fault), or represents a recent change in slip sense.

Footwall stratigraphic units consist of folded Plio-Pleistocene alluvial deposits with growth strata (QP1-QP3) overlain by fluvial terraces (Figs. 3 and 4). Basal green lacustrine mudstone in QP1 dips 25-22°NW. Alluvial cross-bedded sands in QP2 dips 15-5°NW above an angular unconformity. Uppermost alluvial fan deposits (QP3) dip 5°NW above a buttress unconformity. Cretaceous–Miocene bedrock east of the BBF is interpreted to be buried by >>100 m of Plio-Pleistocene sediments as identified from seismic data in neighboring sites in the San Joaquin Valley (Krug et al., 1992; Sterling, 1992; Unruh and Hitchcock, 2015).

The blind San Joaquin fault (SJF) parallels the structural trend of the BBF along the Diablo Range mountain front for as much as ~85 km to the southeast (Figs. 1 and 2a). SJF is defined in the field by a fault-related monocline and anticlinal fold within Plio-Pleistocene and alluvial terrace units (Figs. 2–4). The SJF is thought to join the BBF, which suggest the BBF–SJF are fault splays that intersect at depth (Figs. 2 and 4). SJF fault geometry is interpreted as a 30–42° SW-dipping blind thrust based on the fold axial trace map pattern and structural cross section constraints (Fig. 3 and 4). In the Lone Tree Creek drainage, deformed Plio-Pleistocene units (QP3) and abandoned fluvial terraces show evidence of a monoclinal folding and fold scarps consistent with an east-vergent blind thrust fault geometry (Figs. 2c, 4 and 6). In Corral Hollow Creek, eastward shallowing of the QP2–QP3 dips, surface warping, and tilted terraces reflect fault-related folding from the SJF (Figs. 2b, 4 and 6).

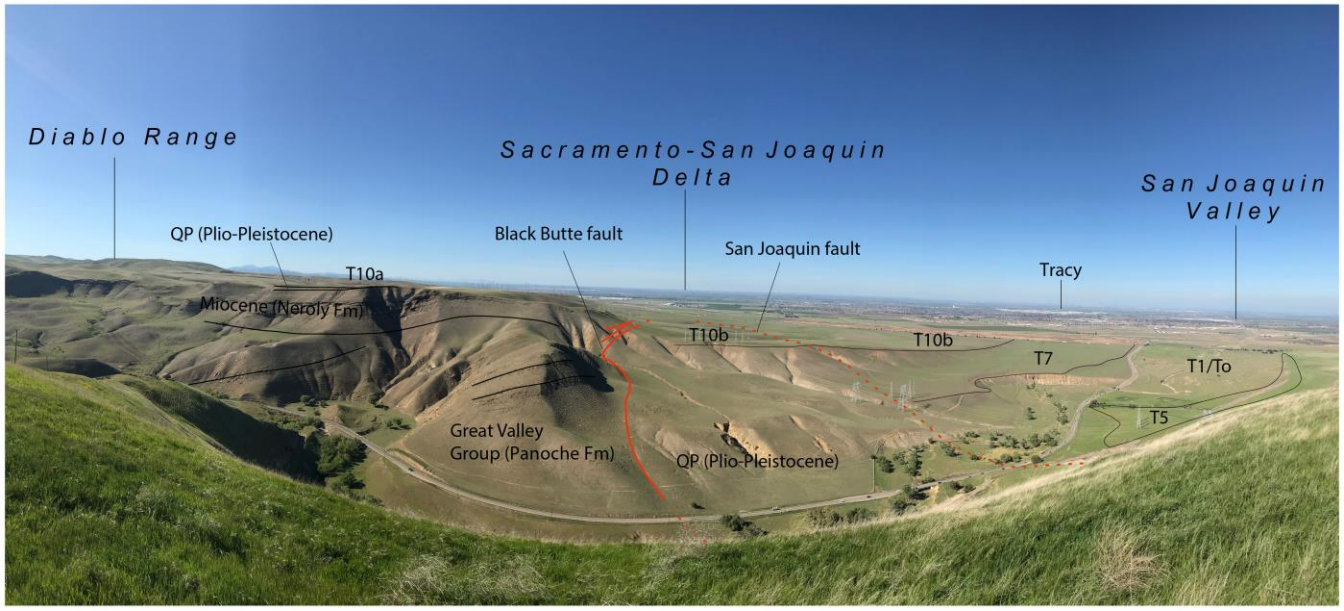

Figure 3. Panoramic view to the north of the Black Butte and San Joaquin faults along Corral Hollow Creek.

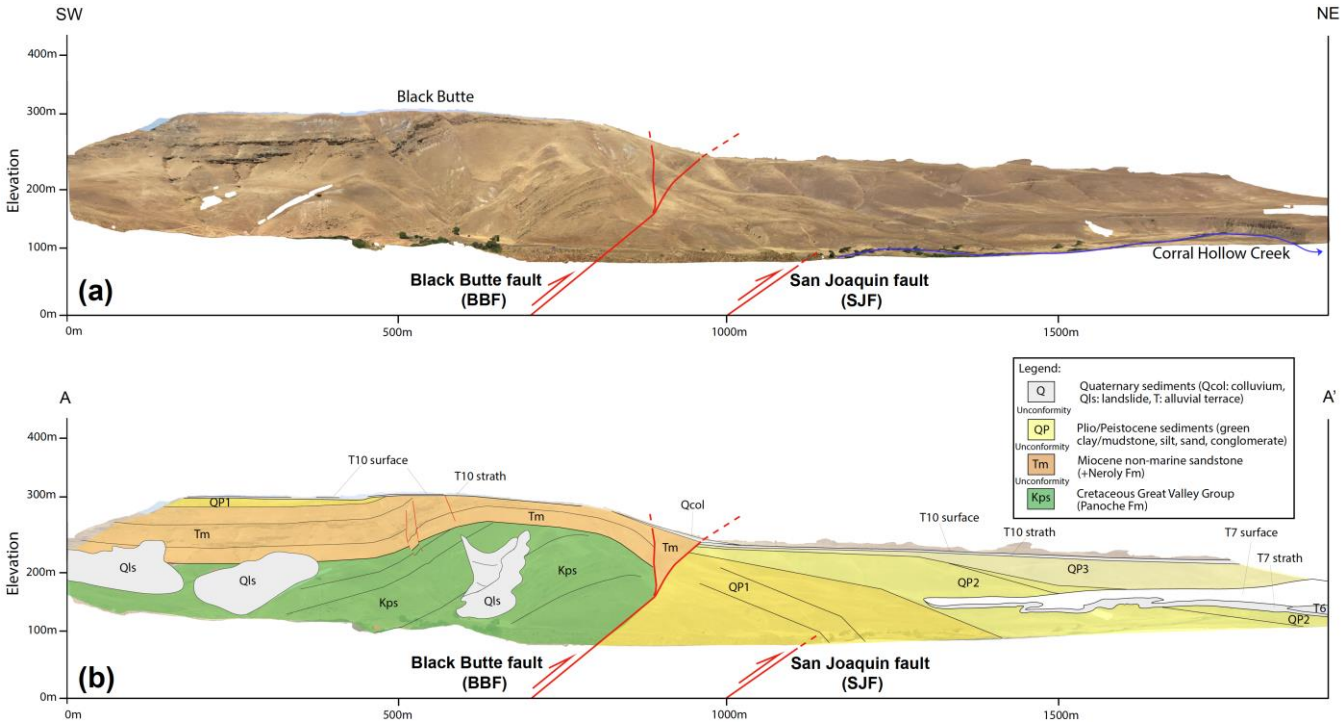

Figure 4. Geologic cross section across the Black Butte fault (BBF) and San Joaquin fault (SJF). **(a)** Upper panel is uninterpreted orthomosaic panoramic photo looking north of Corral Hollow Creek. **(b)** Lower panel is cross section interpretation based on panoramic photolog. See Figure 2a for transect location A-A'.

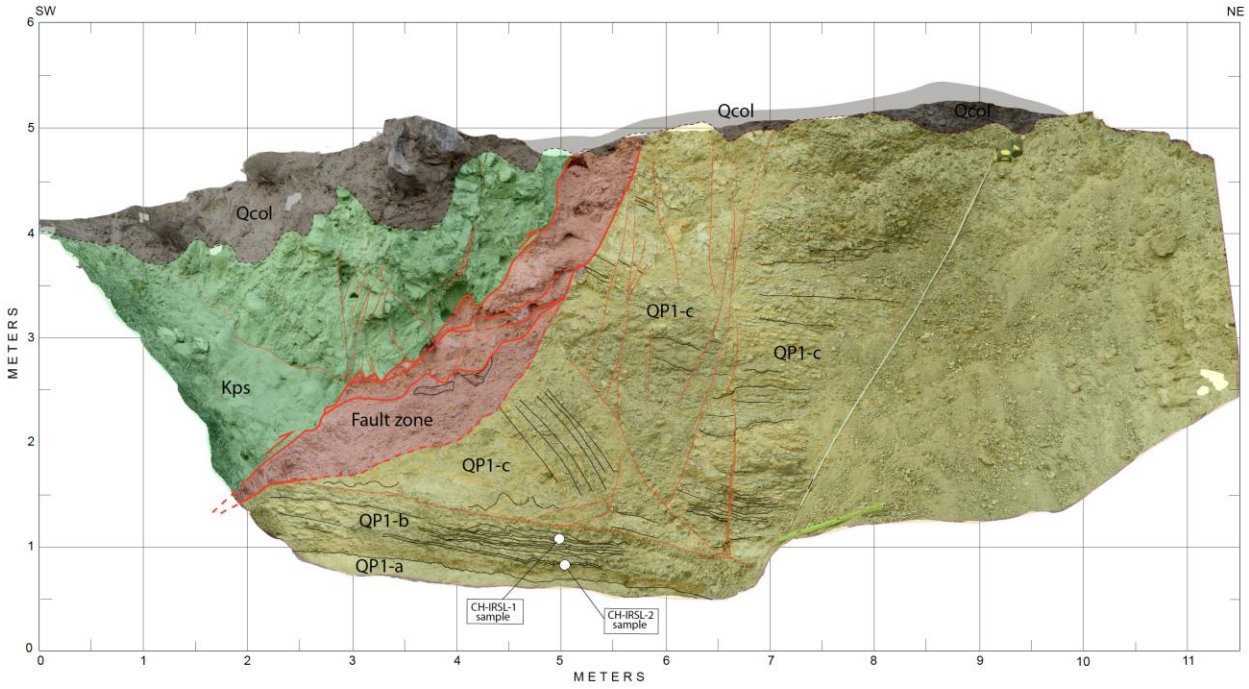

Figure 5. Simplified photolog of a footwall fault splay of the Black Butte fault (BBF) at a gully cut-back exposure that exhibits a ~40°SW dipping fault zone. See Figure 2a for location. Kps: Upper Cretaceous Great Valley Group micaceous-rich sandstone (Panoche Fm); Fault zone: Brecciated siltstone, mudstone, and sandstone, and clay gouge along fault planes; QP1-a: Plio-Pleistocene white sub-arenite fine grained sandstone; QP1-b: Plio-Pleistocene dark purple, brown, orange laminated to thin bedded siltstone, mudstone, and fine-grained sandstone; QP-1c: Deformed and fractured undifferentiated QP1.

GEOMORPHOLOGY AND QUATERNARY MAPPING

Corral Hollow Creek and Lone Tree Creek basins

The study sites are located in the piedmont foothills of the eastern Diablo Range and the Corral Hollow Creek and Lone Tree Creek drainages located south of the latitude of Tracy–Livermore (Fig. 1). These eastward flowing drainages are sourced exclusively from the Diablo Range, draining ~1000 m of relief along the eastern slopes of the range. Lithology exposed within these watersheds include Jurassic–Cretaceous Franciscan (low-grade metasediments), Cretaceous Great Valley Group (marine sediments), and Miocene to Quaternary units (marine to terrestrial sediments) (Figs. 1 and 2a). Drainage patterns are primarily characterized by narrow valleys with intermittent meandering bedrock-alluvial streams within the mountain range; multiple flights of incised fluvial strath terraces best-preserved towards the mountain front; and low gradient ephemeral streams that merge with San Joaquin Valley sediments (Figs. 2a and 3).

The Corral Hollow Creek catchment has ~200 m relief between the highest surfaces and the modern channel, a narrow canyon with bedrock channel, and a stream knickpoint near the BBF fault trace (Figs. 2a and 6). Downstream of the BBF, the valley is wider, has a lower channel gradient, and multiple abandoned strath terraces <5–8 m-thick capping deposits (Figs. 6 and 7). At the drainage outlet with the valley floor, the bedrock channel is covered by unknown thickness of

fluvial to alluvial deposits. A topographic step and fault scarps define the fault trace of the BBF, whereas the SFJ is visible only as a fold scarp or break in surface slope gradient (Figs. 2b, and 6).

In the Lone Tree Creek drainage, the channel is similarly characterized by a thin sedimentary cover across the BBF and SJF, lower relief, and valley incision (~100 m; Figs. 2a, 2c and 6). A topographic step and possible knickpoint at the mountain front in the Lone Tree Creek suggest the SJF is shallower structure at this locality than in the Corral Hollow Creek.

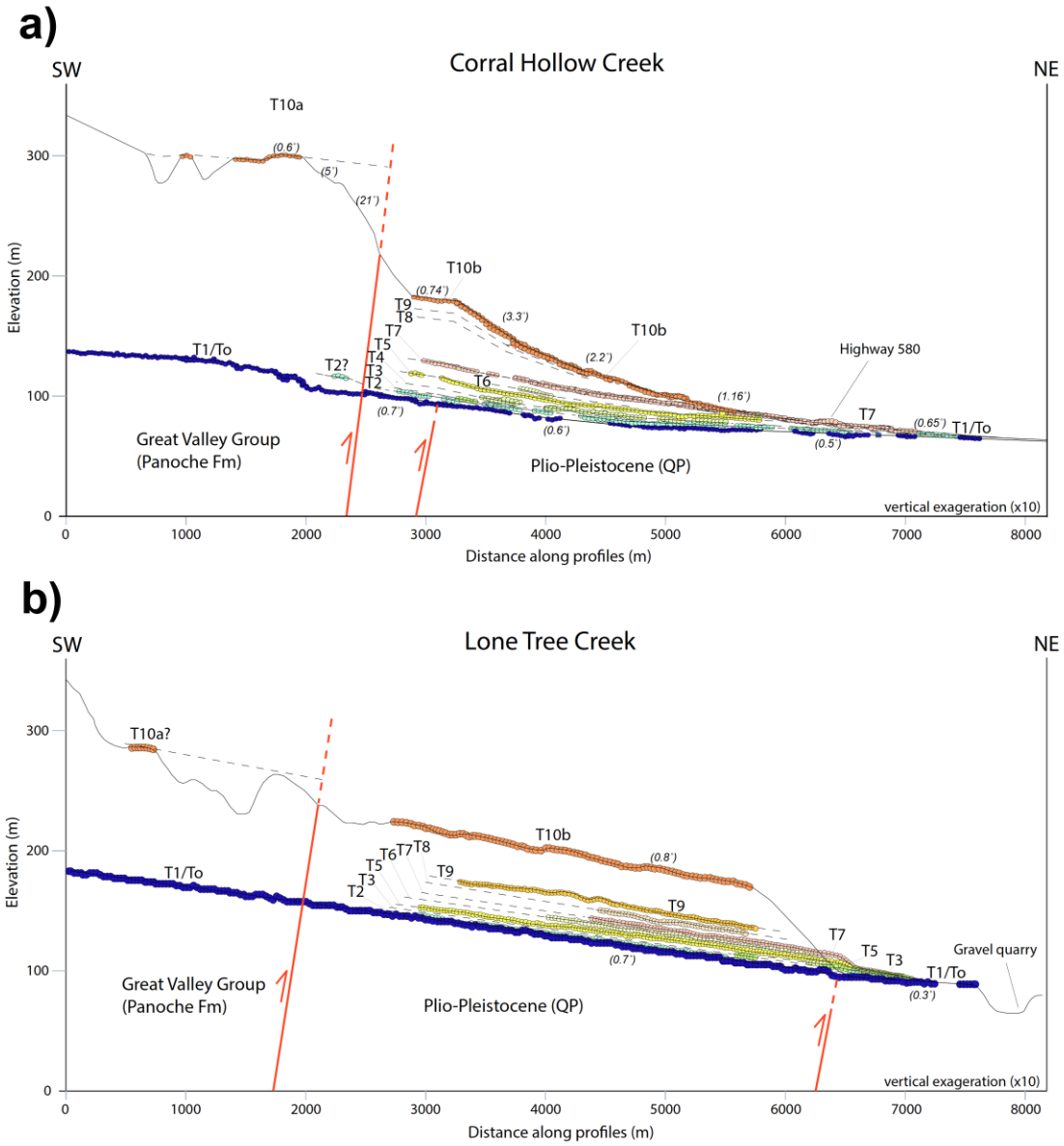

Figure 6. Terrace profiles along Corral Hollow Creek **(a)** and Lone Tree Creek **(b)** across the Black Butte fault (BBF) and San Joaquin fault (SJF). See Figure 2 for terrace chronology. T10 and active channel slope gradients in parentheses. Note vertical exaggeration is x10, including for fault dips and slope gradients. Topographic data are measured from multiple slope profiles using 10m DEM.

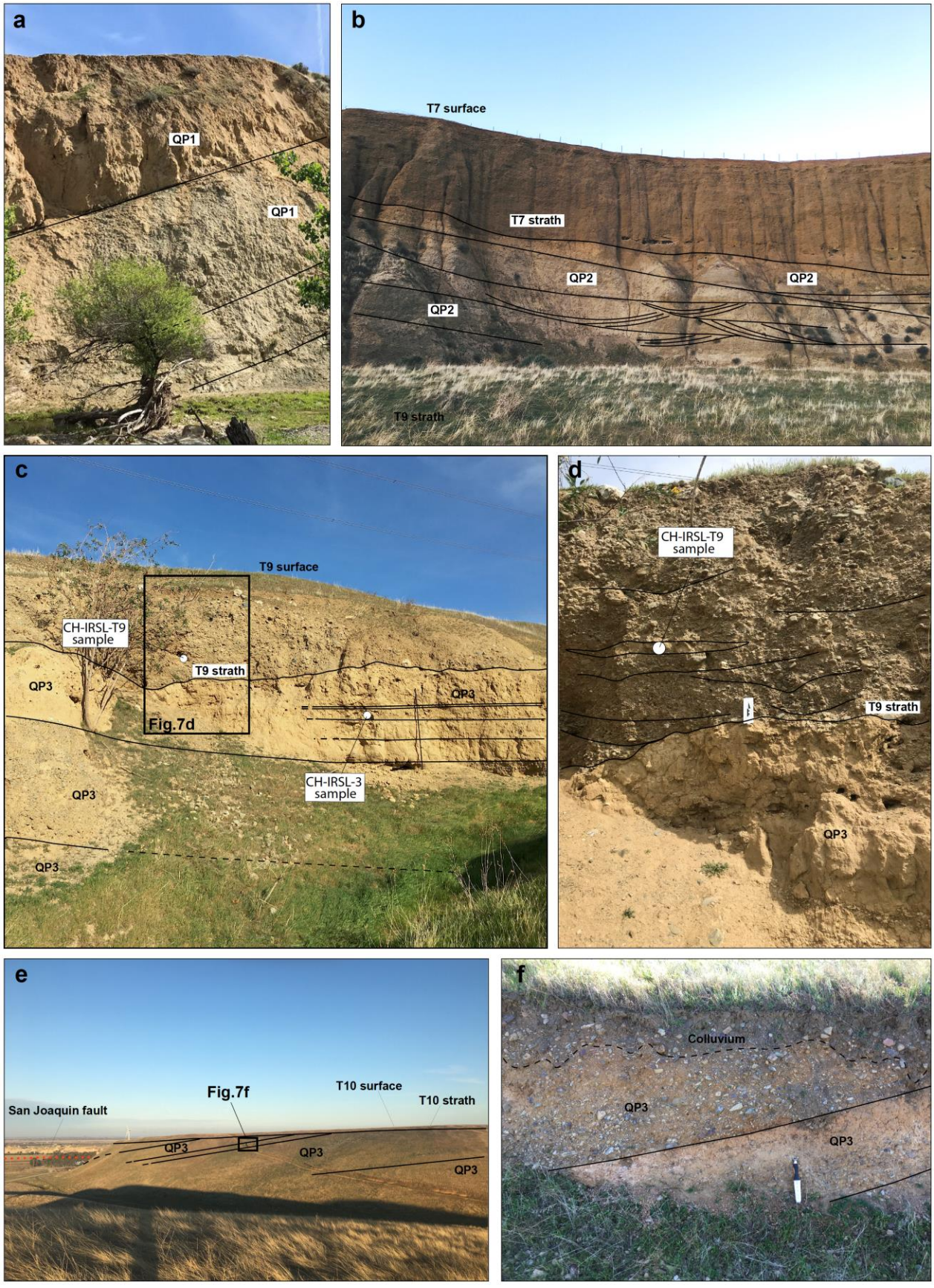
a
QP1
QP1
b
T7 surface
T7 strath
QP2
QP2
QP2
T9 strath
c
T9 surface
CH-IRSL-T9 sample
T9 strath
QP3
QP3
Fig.7d
CH-IRSL-3 sample
QP3
QP3
d
CH-IRSL-T9 sample
T9 strath
QP3
e
Fig.7f
T10 surface
T10 strath
San Joaquin fault
QP3
QP3
QP3
f
Colluvium
QP3
QP3

Figure 7. Field photographs of Plio-Pleistocene units (QP), terraces and sampling locations. **a)** View looking to the south of QP1 exposed along stream level of Corral Hollow Creek. QP1 deposits include a distinctive green mudstone unit and are tilted ~20° to NE. **b)** View to the north along Corral Hollow Creek of QP2 alluvial gravels and sands underlying T7 with a strath contact and angular unconformity. QP2 is titled 10-15° to the NE and the T7 strath and surface slopes are sub-horizontal. **c-d)** View to the east and close-up of a natural exposure of uppermost QP3 underlying T9 south of Corral Hollow Creek. Upper QP3 deposits include thin bedded laminated mudstone and siltstone, structureless silt beds, and intercalations of poorly sorted gravels. T9 terrace deposits consist of imbricated gravels in lenticular beds, fining upward sequences of gravels and sand in channel lenses. IRSL sample locations are shown. **e-f)** View to the east south of Lone Tree Creek of T10 overlying tilted QP3 with a strath contact and angular unconformity. QP3 is tilted 15-20° to the east and T10 strath and surface slopes are sub-horizontal.

Terraces

The Corral Hollow Creek and Lone Tree Creek study sites both exhibit 10 well-preserved strath terraces (T10–T1) (Fig. 2a). Terrace correlation between Corral Hollow and Lone Tree are based on the new age data, soil development, and similar relative terrace elevation to the modern channel within each basin. Terrace mapping and correlation utilized a combination of high-resolution imagery (Lidar, UAV drone photogrammetry, 10 m NED DEM, and 5 m STEREO), multiple topographic profiles, strath exposures, terrace alluvial stratigraphy, and soil development. The terraces are formed on tilted and folded Cretaceous to Plio-Pleistocene units across the BBF, and Plio-Pleistocene units across the SJF, as exposed from natural exposures and soil pits (Figs. 7–9). Many of the terraces form kilometer-long treads with relatively thin terrace gravel caps (1–8 m), bedrock straths, and angular unconformities to underlying bedrock. West of the mountain front, a prominent high surface (T10) is deeply incised and offset across the BBF, while terraces between the BBF and SJF have progressive shallower slope gradients from T10 to T1 merging into the San Joaquin Valley base level (Fig. 6). East of the mountain front, terrace surfaces broaden and merge with San Joaquin valley deposits that bury underlying bedrock or Plio-Pleistocene sediments (Figs. 2a and 4).

T10 represents the highest and most incised mapped surface and correlates with a lateral extensive surface deposit across the eastern Diablo Range foothills (Fig. 2). Terrace stratigraphy is characterized by moderate to poorly sorted grain-dominated gravels, weakly developed clast imbrication within lenticular bed geometry, and few sand rich layers (Figs. 8 and 9). Map relations and sediment architecture suggest T10 alluvial stream formation either overlapped or capped broad coalescent alluvial fans deposits of the uppermost tilted Plio-Pleistocene units (see section on Plio-Pleistocene units). Soils are well developed with dark brown to brownish red weathering color, 1–1.5 m thick clay rich accumulation horizons (Bt), and deep pedogenic carbonate soil horizons (Bk, Bkm, Bkt) extending to >2 m depth into terrace deposit (Figs 8 and 9; Table 1). In Corral Hollow Creek, T10 occupies an elevation of ~300 m relative to the modern channel, is characterized by a 0.6°E-sloping surface, and thin (1–3 m) capping gravels unconformably overlie tilted 5°WSW Plio-Pleistocene units and 5–25°WSW Miocene bedrock units (Figs. 3–6). In the BBF footwall, T10 occupies elevation between 190m and 100m relative to the modern channel and is offset surface across the fault based on map relations, similar slope gradient (0.7°E), terrace stratigraphy, and degree of soil development. Further south in the Lone Tree Creek, T10 terraces in the BBF hanging wall and footwall occupy similar elevations to those exposed in Corral Hollow Creek, but are poorly preserved, highly eroded surfaces beveled onto Cretaceous–Miocene bedrock (Figs. 2a and 6).

Sequentially lower terraces T9–T1 progressively step down from T10 to the modern channel in both Corral Hollow and Lone Tree Creeks (Fig. 2 and 6). Terrace profiles reveal slope breaks, warped surfaces, and fold scarps above the projection of the SJF. East of the SJF, terrace surfaces show tilting where slope gradients progressively decrease from west to east towards the San Joaquin Valley (Fig. 6). Terrace deposit thickness ranges from 1.5 and 8 m and unconformably overlie Plio-Pleistocene deposits (Figs. 7–9). In contrast to T10, T9–T1 terrace deposits are characterized by moderate to well sorted gravel beds; well-developed clast imbrication indicating paleoflow to the east in multiple lenticular beds, multiple 10–30 cm thick cross-bedded to laminated sand-rich channel lenses, and a fine-grained cap (Figs. 8–9). Terrace and soil deposits are rich in silt indicating no clear depth relationship. Primary source of silt is likely from recycled eolian material that form part of the Pliocene-Pleistocene alluvial fan sequence. Pedogenic clay accumulation and soil color are concentrated in the uppermost terrace deposits (1–1.5 m). Overall soil development decreases with relative terrace age observed from weathering soil color (dark brown to yellowish gray), decreasing depth of the pedogenic clay accumulation horizons (Bt to Bw), and lower proportions of weathered clasts (Figs. 8 and 9; Table 1). Stage I–III carbonate horizons are well developed throughout most of the terraces with little correlation to relative terrace age, suggesting rapid pedogenic carbonates formation after terrace abandonment (Sowers et al., 2000).

TABLE 1. Soil analytical data of depth profiles at Corral Hollow and Lone Tree terraces.

Depth profile				Horida soil data (grain size)				Loss on ignition (LOI) soil data							
Sample	Depth (cm)	Munsell color	General color	%<2microns (clay)	%2-50 microns (silt)	%50-2000 microns (sand)	Soil texture	% H_20	% Org.	% Carb.	% Non Carb. Mineral	Dry Density (g/cm3)	Wet Density (g/cm3)	Ratio Dry/Wet	Ratio Org/Wet
Corral Hollow Terraces															
T10 Upper - BBF hangingwall															
CH-T10UP-10	-10	10YR 4/2	pale brown	30.8	63.7	5.5	silty clay loam	2.3	6.1	10.1	83.8	1.9	1.9	1.0	0.1
CH-T10UP-20	-20	10YR 3/2	dark brown	22.7	70.3	7.0	silt loam	3.3	5.0	7.7	87.2	1.9	2.0	1.0	0.0
CH-T10UP-26	-26	10YR 4/2	pale brown-gray	30.3	62.6	7.1	silty clay loam	2.7	5.9	11.0	83.1	1.9	1.9	1.0	0.1
CH-T10UP-36	-36	10YR 4/2	pale brown	29.7	62.5	7.8	silty clay loam	3.6	5.3	13.1	81.7	1.8	1.9	1.0	0.1
CH-T10UP-40	-40	10YR 3/2	medium brown-gray	32.2	59.9	8.0	silty clay loam	4.6	4.7	9.7	85.6	1.9	2.0	1.0	0.0
CH-T10UP-60	-60	10YR 4/2	medium brown	37.0	51.8	11.3	silty clay loam	6.0	4.2	9.4	86.4	1.8	2.0	0.9	0.0
CH-T10UP-70	-70	2.5Y 5/2	pale brown-gray	34.2	63.9	1.9	silty clay loam	3.9	5.6	16.4	78.0	1.8	1.8	1.0	0.1
CH-T10UP-80	-80	7.5YR 5/3	pale brown-gray-red	31.5	61.0	7.5	silty clay loam	4.1	5.3	12.4	82.3	1.8	1.9	1.0	0.1
CH-T10UP-90	-90	7.5YR 4/3	medium brown-red	38.3	57.4	4.3	silty clay loam	4.6	4.0	7.6	88.3	1.9	2.0	1.0	0.0
T10 South - BBF footwall															
CH-T10S-10	-10	10YR 3/2	dark brown	37.1	55.1	7.9	silty clay loam	6.2	6.5	6.7	86.7	1.8	1.9	0.9	0.1
CH-T10S-20	-20	7.5YR 3/2	dark greyish brown	38.7	59.3	2.0	silty clay loam	7.8	4.9	6.9	88.2	1.8	1.9	0.9	0.0
CH-T10S-40	-40	7.5YR 3/2	dark brown	41.1	53.6	5.4	silty clay	6.9	4.7	6.7	88.6	1.8	2.0	0.9	0.0
CH-T10S-60	-60	7.5YR 3/2	dark brown	28.4	65.2	6.4	silty clay loam	6.4	4.9	6.9	88.2	1.8	1.9	0.9	0.0
CH-T10S-80	-80	7.5YR 3/2	dark brown	41.6	55.1	3.2	silty clay	8.5	4.6	7.5	87.9	1.8	1.9	0.9	0.0
CH-T10S-100	-100	10YR 4/3	dark brown	38.2	58.5	3.3	silty clay loam	9.3	4.4	8.7	87.0	1.7	1.9	0.9	0.0
CH-T10S-120	-120	7.5YR 4/3	redish brown	42.1	57.9	0.0	silty clay	8.8	4.2	6.8	89.0	1.8	1.9	0.9	0.0
CH-T10S-140	-140	7.5YR 5/4	pale yellowish brown	28.6	68.8	2.6	silty clay loam	6.8	4.6	12.9	82.5	1.7	1.9	0.9	0.0
CH-T10S-160	-160	7.5YR 5/6	dark yellowish brown	18.7	67.3	14.0	silt loam	6.5	3.5	5.1	91.4	1.9	2.0	0.9	0.0
CH-T10S-180	-180	10YR 5/4	dark yellowish brown	9.1	66.6	24.3	silt loam	4.3	2.9	3.8	93.2	2.1	2.2	1.0	0.0
CH-T10S-200	-200	10YR 5/4	brown	16.0	73.1	10.9	silt loam	5.5	2.6	3.7	93.7	2.0	2.1	0.9	0.0
CH-T10S-220	-220	10YR 5/4	yellowish brown	9.4	58.0	32.6	silt loam	2.0	2.2	2.7	95.2	2.2	2.3	1.0	0.0
CH-T10S-240	-240	7.5YR 5/6	yellowish brown	17.8	80.4	1.9	silt loam	5.6	2.6	3.7	93.7	2.0	2.1	0.9	0.0
T7															
CH-T7-10	-10	7.5YR 3/2	brown	35.4	57.3	7.3	silty clay loam	2.3	4.1	4.5	91.4	2.1	2.1	1.0	0.0
CH-T7-30	-30	7.5YR 4/3	yellowish brown	37.6	54.8	7.6	silty clay loam	1.4	5.4	5.3	89.3	2.0	2.1	1.0	0.1
CH-T7-50	-50	10YR 4/3	yellowish brown	49.0	48.6	2.4	silty clay	2.6	5.6	8.0	86.4	1.9	2.0	1.0	0.1
CH-T7-70	-70	10YR 4/3	yellowish brown	34.6	58.6	6.8	silty clay loam	1.5	4.2	4.4	91.5	2.1	2.1	1.0	0.0
CH-T7-90	-90	10YR 4/3	yellowish brown	48.8	50.7	0.5	silty clay	3.2	4.5	8.8	86.8	1.9	2.0	1.0	0.0
CH-T7-110	-110	10YR 4/3	yellowish brown	52.9	47.1	0.0	silty clay	1.4	3.3	3.7	93.0	2.2	2.2	1.0	0.0
CH-T7-130	-130	10YR 4/3	yellowish brown	42.0	57.8	0.2	silty clay	1.7	4.0	4.5	91.5	2.1	2.1	1.0	0.0
CH-T7-150	-150	2.5Y 6/3	pale brown	21.6	60.4	18.0	silt loam	0.5	2.4	9.1	88.5	2.2	2.2	1.0	0.0
CH-T7-205	-205	2.5Y 6/3	pale brown	46.0	54.0	0.0	silt clay	1.2	3.0	7.4	89.6	2.1	2.2	1.0	0.0
T4															
CH-T4-10	-10	2.5Y 3/2	greyish brown	29.6	60.0	10.4	silty clay loam	1.9	3.9	4.5	91.6	2.1	2.1	1.0	0.0
CH-T4-30	-30	2.5Y 4/2	brown	30.0	58.5	11.5	silty clay loam	2.7	3.7	5.2	91.1	2.1	2.1	1.0	0.0
CH-T4-50	-50	2.5Y 3/2	reddish brown	28.6	58.7	12.7	silty clay loam	3.6	3.5	4.4	92.1	2.1	2.1	1.0	0.0
CH-T4-70	-70	2.5Y 4/3	light yellowish brown	28.8	56.7	14.5	silty clay loam	3.9	3.6	4.6	91.8	2.0	2.1	1.0	0.0
CH-T4-90	-90	10YR 4/3	light brown	29.3	60.0	10.7	silty clay loam	2.8	3.6	4.3	92.1	2.1	2.1	1.0	0.0
CH-T4-105	-105	10YR 4/3	orangish brown	32.9	60.6	6.5	silty clay loam	4.0	3.2	3.6	93.3	2.1	2.2	1.0	0.0
CH-T4-125	-125	10YR 4/3	orangish brown	26.5	73.4	0.2	silt loam	3.6	3.3	3.4	93.3	2.1	2.2	1.0	0.0
CH-T4-145	-145	10YR 4/3	orangish brown	22.2	76.3	1.5	silt loam	2.5	3.0	2.9	94.1	2.2	2.2	1.0	0.0
CH-T4-165	-165	10YR 5/4	yellowish brown	34.5	62.5	3.0	silty clay loam	0.9	2.3	2.5	96.8	2.4	2.4	1.0	0.0
CH-T4-185	-185	2.5Y 5/3	pale brown	23.2	63.6	13.1	silt loam	1.6	1.6	1.7	95.2	2.3	2.3	1.0	0.0
CH-T4-205	-205	10YR 4/3	yellowish brown	46.3	53.7	0.0	silt clay	1.3	1.7	1.9	96.4	2.3	2.4	1.0	0.0
CH-T4-235	-235	10YR 4/3	yellowish brown	43.7	50.6	5.7	silty clay	3.6	2.6	3.7	93.7	2.1	2.2	1.0	0.0
T3															
CH-T3-10	-10	10YR 4/3	brown	24.6	58.4	16.9	silt loam	2.7	3.1	4.3	92.6	2.1	2.2	1.0	0.0
CH-T3-30	-30	2.5Y 3/2	brown	27.0	59.9	13.1	silt loam	3.7	4.3	4.1	91.6	2.0	2.1	1.0	0.0
CH-T3-50	-50	7.5YR 3/2	medium-dark brown	26.4	60.0	13.6	silt loam	4.0	3.4	4.0	92.6	2.0	2.1	1.0	0.0
CH-T3-70	-70	7.5YR 3/2	brown	27.3	64.0	8.7	silt loam	7.1	3.7	4.0	92.3	1.9	2.0	0.9	0.0
CH-T3-90	-90	7.5YR 3/2	brown	25.3	59.0	15.7	silt loam	7.2	3.7	3.8	92.5	1.9	2.0	0.9	0.0
CH-T3-110	-110	10YR 3/2	yellowish brown	25.2	70.2	4.6	silt loam	3.2	2.8	3.2	94.0	2.1	2.2	1.0	0.0
CH-T3-130	-130	10YR 3/2	yellowish brown	25.4	63.6	10.9	silt loam	1.8	2.1	2.3	95.7	2.3	2.3	1.0	0.0
CH-T3-150	-150	2.5Y 5/3	yellowish brown	22.0	67.1	10.9	silt loam	2.2	1.8	2.0	96.2	2.3	2.3	1.0	0.0
CH-T3-170	-170	2.5Y 4/3	pale brown (mixed)	24.3	59.6	16.0	silt loam	0.8	1.3	1.7	97.0	2.4	2.4	1.0	0.0
T2 Upper															
CH-T2-UP-10	-10	2.5Y 4/3	brown	22.7	58.4	18.9	silt loam	2.7	3.6	3.4	93.0	2.1	2.2	1.0	0.0
CH-T2-UP-30	-30	2.5Y 4/3	brown	22.4	57.3	20.3	silt loam	2.3	3.2	3.4	93.5	2.2	2.2	1.0	0.0
CH-T2-UP-50	-50	2.5Y 3/2	brown	22.6	57.8	19.6	silt loam	3.6	3.3	3.3	93.4	2.1	2.2	1.0	0.0
CH-T2-UP-70	-70	7.5YR 3/2	brown	21.7	61.7	16.6	silt loam	4.4	3.1	3.3	93.6	2.1	2.2	1.0	0.0
CH-T2-UP-90	-90	2.5Y 4/2	brown	22.8	57.6	19.6	silt loam	2.3	3.0	3.1	93.9	2.2	2.2	1.0	0.0
CH-T2-UP-120	-120	10YR 5/3	brown	41.3	58.7	0.0	silty clay	3.0	2.7	3.1	94.2	2.2	2.2	1.0	0.0
CH-T2-UP-140	-140	10YR 5/3	light brown	30.8	57.1	12.1	silty clay loam	2.0	2.1	2.3	95.6	2.3	2.3	1.0	0.0
CH-T2-UP-150	-150	2.5Y 5/3	light brown	27.2	65.8	7.0	silt loam	1.7	1.6	1.8	96.6	2.3	2.4	1.0	0.0
CH-T2-UP-170	-170	10YR 5/3	light brown	19.6	58.7	21.8	silt loam	1.0	1.3	2.3	96.4	2.4	2.4	1.0	0.0
T2 Lower															
CH-T2-UP-4	-4	10YR 4/2	med-dark brown	6.9	40.6	52.5	sandy loam	3.5	12.5	2.9	84.6	1.7	1.7	1.0	0.1
CH-T2-UP-10	-10	2.5Y 4/2	med-dark brown	20.0	54.6	25.4	silt loam	1.6	2.9	2.6	94.5	2.2	2.3	1.0	0.0
CH-T2-UP-200	-20	2.5Y 4/3	med-dark brown	21.4	56.3	22.2	silt loam	2.0	2.5	2.7	94.8	2.2	2.3	1.0	0.0
CH-T2-UP-30	-30	7.5YR 3/2	med-dark brown	21.6	49.8	28.7	loam	2.2	2.4	2.7	94.9	2.2	2.3	1.0	0.0
CH-T2-UP-40	-40	2.5Y 4/2	med-dark brown	20.5	53.9	25.6	silt loam	2.1	2.4	2.9	94.7	2.2	2.3	1.0	0.0
CH-T2-UP-60	-60	2.5Y 4/2	med-dark brown	16.0	50.8	33.3	silt loam	2.0	2.5	2.7	94.8	2.2	2.3	1.0	0.0
CH-T2-UP-80	-80	10YR 4/2	light brown	23.1	60.2	16.7	silt loam	1.4	2.0	2.4	95.6	2.3	2.3	1.0	0.0
CH-T2-UP-100	-100	10YR 4/3	pale brown	22.5	58.0	19.5	silt loam	1.4	1.5	1.9	96.6	2.3	2.4	1.0	0.0
CH-T2-UP-120	-120	10YR 5/3	pale brown	22.1	61.8	16.2	silt loam	0.8	1.7	2.3	96.1	2.4	2.4	1.0	0.0
CH-T2-UP-140	-140	10YR 5/3	pale brown	24.7	57.5	17.8	silt loam	0.7	1.7	3.4	94.9	2.3	2.3	1.0	0.0
CH-T2-UP-160	-160	10YR 5/3	pale brown	25.1	63.3	11.5	silt loam	0.9	1.8	4.4	93.8	2.3	2.3	1.0	0.0
CH-T2-UP-180	-180	10YR 5/3	pale brown	34.0	62.9	3.2	silty clay loam	1.4	2.1	4.8	93.0	2.2	2.3	1.0	0.0
CH-T2-UP-200	-200	10YR 4/3	light greyish brown	41.9	58.1	0.0	silty clay	0.9	1.6	3.8	94.6	2.3	2.3	1.0	0.0
CH-T2-UP-230	-230	10YR 4/3	light organish brown	43.1	56.9	0.0	silty clay	1.6	1.4	2.4	96.2	2.3	2.4	1.0	0.0
Lone Tree Terraces															
T10 North															
LTR-T10N-35	-35	5YR4/4	reddish brown	33.5	60.9	5.6	silty clay loam	4.6	2.1	10.8	87.19	1.98	2.07	0.95	0.02
LTR-T10N-55	-55	5YR 4/4	reddish brown	38.3	50.5	11.3	silty clay loam	5.2	1.7	13.6	84.70	1.93	2.03	0.95	0.02
LTR-T10N-90	-90	5YR 4/4	reddish brown	35.8	54.5	9.8	silty clay loam	5.9	1.6	14.8	83.60	1.88	2.00	0.94	0.02
LTR-T10N-135	-135	5YR 4/6	yellowish red	38.2	53.0	8.9	silty clay loam	5.0	1.3	12.7	85.97	1.96	2.07	0.95	0.01
LTR-T10N-180	-180	7.5YR 6/6	reddish yellow	27.0	60.0	13.0	silty loam	1.6	1.6	5.9	92.52	2.23	2.27	0.98	0.02
T10 South															
LTR-T10S-20	-20	10YR 3/2	very dark grayish brown	40.9	50.2	8.9	silty clay	3.6	2.0	9.0	88.95	2.05	2.13	0.96	0.02
LTR-T10S-55	-55	7.5YR 3/4	dark brown	40.5	56.3	3.2	silty clay	4.4	1.6	10.4	87.92	2.01	2.10	0.96	0.02
LTR-T10S-85	-85	5YR 5/6	yellowish red	26.5	68.3	5.2	silty loam	3.8	2.2	11.0	86.74	2.00	2.08	0.96	0.02
LTR-T10S-130	-130	7.5YR 5/6	strong brown	33.3	64.8	1.9	silty clay loam	2.3	1.7	5.5	92.82	2.20	2.25	0.98	0.02
LTR-T10S-185	-185	7.5YR 4/6	strong brown	38.2	57.7	4.1	silty clay loam	3.0	1.9	5.4	92.69	2.16	2.22	0.97	0.02
T9															
LTR-T9-25	-25	5YR 5/6	yellowish red	17.7	57.8	24.5	silt loam	0.9	2.0	4.2	93.77	2.28	2.30	0.99	0.02
LTR-T9-60	-60	5YR 4/4	reddish brown	37.6	58.1	4.3	silty clay loam	8.0	2.9	9.2	87.96	1.82	1.98	0.92	0.03
LTR-T9-80	-80	5YR 5/8	yellowish red	7.3	31.0	61.7	sandy loam	5.5	2.6	8.9	88.53	1.94	2.06	0.94	0.02
T7															
LTR-T7-30	-30	7.5YR 4/6	strong brown	15.2	63.3	21.5	silt loam	1.1	1.9	3.7	94.44	2.29	2.32	0.99	0.02
LTR-T7-60	-60	5YR 4/4	reddish brown	33.0	52.7	14.3	silty clay loam	3.8	2.7	6.4	90.91	2.06	2.14	0.96	0.03
LTR-T7-110	-110	7.5YR 4/4	brown	24.8	67.4	7.8	silt loam	0.9	1.5	3.3	95.12	2.33	2.36	0.99	0.02
LTR-T7--160	-160	10YR 7/4	very pale brown	49.3	50.7	0.0	silty clay	0.6	1.6	6.8	91.65	2.27	2.28	0.99	0.02
T6															
LTR-T6-25	-25	10YR 5/4	yellowish brown	17.8	59.2	23.0	silt loam	1.1	2.1	4.4	93.50	2.26	2.29	0.99	0.02
LTR-T6-45	-45	10YR 5/4	yellowish brown	16.8	61.6	21.6	silt loam	1.2	2.0	4.1	93.90	2.27	2.29	0.99	0.02
LTR-T6-65	-65	7.5YR 4/6	strong brown	39.6	60.4	0.0	silty clay loam	1.6	2.0	4.3	93.70	2.24	2.28	0.98	0.02
LTR-T6-140	-140	10YR 6/6	brownish yellow	14.3	77.0	8.7	silt loam	3.8	2.1	9.5	88.36	2.03	2.11	0.96	0.02
T5															
LTR-T5-25	-25	7.5YR 5/4	brown	17.2	63.0	19.9	silt loam	1.0	2.0	5.0	93.01	2.26	2.28	0.99	0.02
LTR-T5-50	-50	10YR 5/6	yellowish brown	17.3	65.0	17.7	silt loam	2.2	1.9	5.5	92.53	2.19	2.24	0.98	0.02
LTR-T5-100	-100	10YR 5/6	yellowish brown	34.4	63.7	1.9	silty clay loam	1.2	1.6	3.8	94.67	2.31	2.33	0.99	0.02
LTR-T5-145	-145	10YR 4/4	dark yellowish brown	16.6	67.9	15.5	silt loam	0.5	1.3	3.0	95.67	2.38	2.39	1.00	0.01

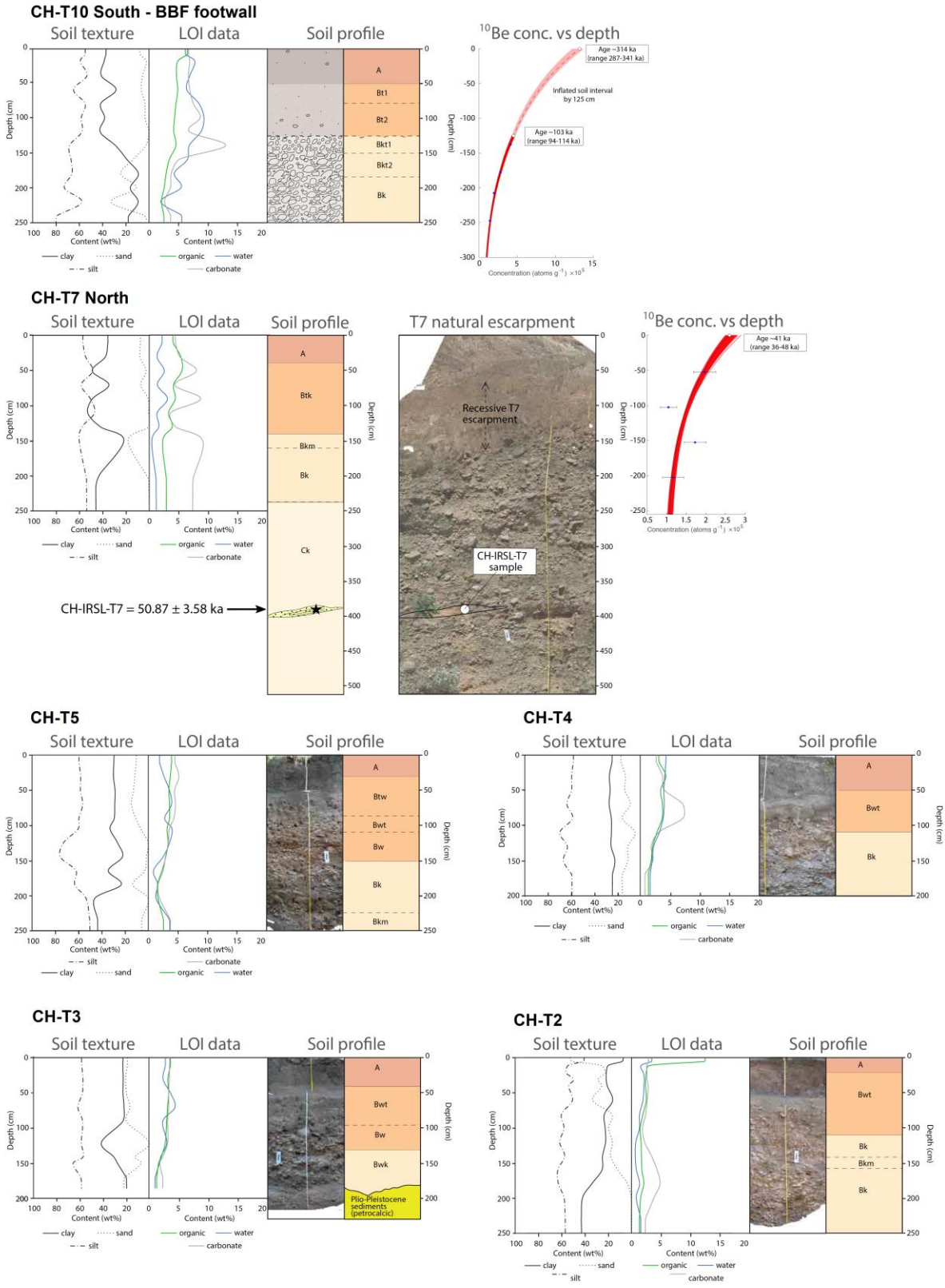

Figure 8. Terrace stratigraphy and soil profile characteristics for terraces T10, T7, T5, T4, T3, and T2 in Corral Hollow Creek study site. Soil pit locations shown in Figure 2a. Left panel shows soil texture plots

for clay, silt, and sand content. Middle panel shows loss-of-ignition (LOI) soil data for organic, water, and carbonate content (inferred attributed to meteoric/pedogenic sources). See Table 1 for complete details. Right panel shows simplified soil horizons with associated field photos. Available TCN ^{10}Be and IRSL age data are shown (see Tables 2 and 3).

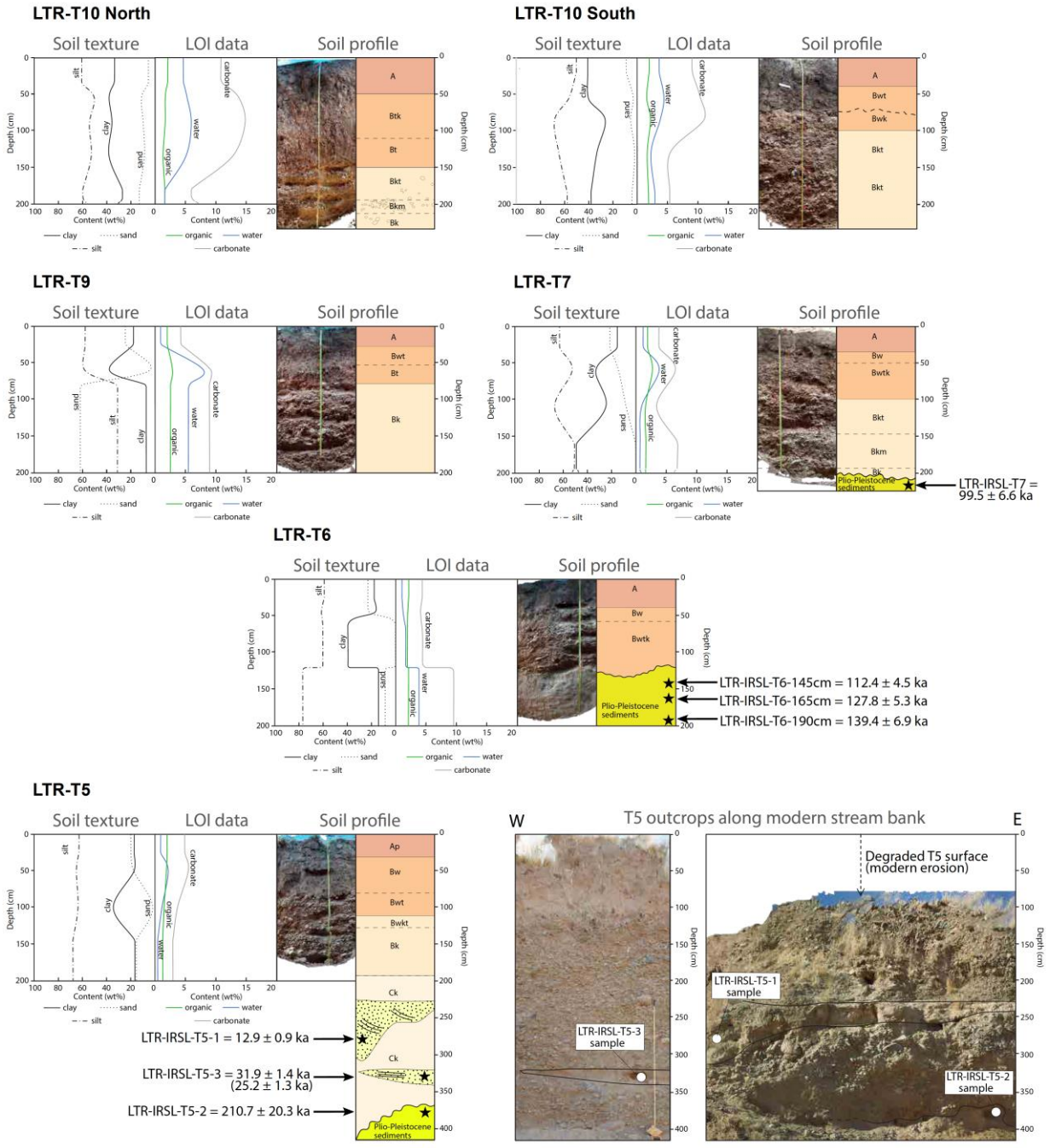

Figure 9. Terrace stratigraphy and soil profile characteristics for terraces T10, T9, T7, T6, and T5 in Lone Tree Creek study site. Soil pit locations shown in Figure 2c. Left panel shows soil texture plots for clay, silt, and sand content. Middle panel shows loss-of-ignition (LOI) soil data for organic, water, and carbonate content (inferred attributed to meteoric/pedogenic sources). See Table 1 for complete details of soil data. IRSL sample locations are shown (see Table 2).

Pliocene-Pleistocene synorogenic sediments (QP1–QP3)

Terraces are etched into older Plio-Pleistocene deposits, as mapped regionally as QP by Diblee (1981a;1981b; Figs. 2a and 4). Previous work along the western edge of the San Joaquin Valley described these >>100 m thick units as coalesced alluvial fan and locally interbedded lacustrine deposits sourced from the Diablo Range or Coast Ranges (Lettis 1982; Unruh and Lettis, 1991). These units correlate with the Tulare Formation (Plio-Pleistocene to >550 ka) and Los Banos Alluvium (535 to 80 ka).

Angular unconformity to disconformity characterizes contacts between sub-horizontal fluvial terrace deposits and underlying folded Plio-Pleistocene deposits (Fig. 3 and 4). In Corral Hollow Creek and Lone Tree Creek, Plio-Pleistocene deposits are subdivided into three units that show progressive shallowing of dip up section from 25° to 5° from west to east, respectively. The stratigraphically lowest unit QP1 at Corral Hollow consists of green mudstone with dips 25–22° to the east (Figs. 4 and 7). They are interpreted as lacustrine deposits similar to the regionally extensive Corcoran Clay member of the Tulare Formation found beneath the San Joaquin Valley (600–800 ka; Lettis 1982 and references therein). An angular unconformity marks the contact between QP1 and the overlying QP2. QP2 dips 5–15° to the east, is characterized by extensively channelized alluvial sand and gravels deposits, meter-sized cross beds with paleoflow to north, northeast, and east (Figs. 4 and 7). Up-section a second angular unconformity marks the contact between QP2 and the overlying QP3, which dips up to 5°. Dip is steeper, 15–25° east, across the SJF in Lone Tree Creek (Fig. 4). QP1 and QP2 are only observed at Corral Hollow Creek, whereas QP3 is observed in both drainages. QP3 is characterized by laterally variable interfingering tan brown to buff yellowish brown thick-bedded structureless silt-rich mudstone, thin bedded sand with cross stratification, laminated fine grain sand, and thick to massive bedded poorly sorted conglomerate (Fig. 7). Although depositional dip can reach 5° in steep alluvial fans, QP3 deposits are indicative of medial to distal on-axis to off-axis low gradient deposition, given the multiple sequences of laminated calcic silt to mudstone facies indicative of lower energy environment with episodic flooding and desiccation (e.g., playa deposits), fine grained distal sand skirts, and thick bedded accumulation of structureless aeolian silt. Both QP2 and QP3 units correlate to the Los Banos Alluvium (535 to 80 ka), recognized as regionally extensive deposits along the eastern the Diablo Range foothills (Lettis 1982; Unruh and Lettis, 1991), which suggest a period of broad alluvial fans development sourced from uplifted highlands in the core of the Diablo Range or Coast Ranges. QP units west of the BBF have been deeply eroded but may be the dominant source of recycled aeolian silt in younger terrace deposits (Figs. 8 and 9).

Overall, the depositional model for the stratigraphic succession of QP1–QP3 is interpreted as progressive angular unconformities and folding, accompanied by coarsening up-section from lacustrine to alluvial fans deposits. Map and stratigraphic evidence indicate QP units are synorogenic growth strata documenting sequential deformation along the Diablo Range foothills since at least 600–800 ka (QP1) to 211–100 ka (QP3; see age results for Plio-Pleistocene units). Structural relations and cross section suggest sustained and coeval deformation between faulting on the BBF, fault-related folding of the SJF, and fault-related incision across the BBF–SJF.

QUATERNARY GEOCHRONOLOGY

Methods

We employed a combination of infrared stimulated luminescence (IRSL), optically luminated luminescence (OSL), and terrestrial cosmogenic nuclide (TCN) methods to date geomorphic surfaces, terrace deposits, as well as underlying Plio-Pleistocene units (QP).

Infrared stimulated luminescence (IRSL) targets grain-sized feldspars and polycrystalline quartz. IRSL provided a more suitable dating method as samples contained significant amount of polycrystalline quartz that lack of sensitivity response to optically stimulated luminesce (OSL). Sampling targets included sand- or silt-rich facies associated with alluvial streams or fluvial deposition most likely to have been reset by sunlight exposure (e.g., Rittenour, 2008; Rhodes, 2011). In the field, samples for IRSL dating were collected by pounding opaque metal pipes into sediment layers and were tightly packed to prevent light exposure and sediment mixing. Samples were sent to the USGS Luminescence Laboratory in Denver for processing to purified feldspar separates. Small 1-mm aliquots (50–100 grains) of medium-grained (125–90 microns) potassium feldspar sand was analyzed using the single-aliquot regenerative-dose (SAR) technique (Murray and Wintle, 2000) on Risø IRSL LED's readers. Stimulation was conducted at 180°C following 230°C preheats (100s) for regenerative and natural doses. IRSL ages were calculated from 15–24 aliquots. Equivalent dose (D_E) values were calculated using both the central age model (CAM) and minimum age model (MAM) of Galbraith and Roberts (2012). In our results, we present final age summary using MAM or CAM, depending on the scatter, in some cases, partial bleaching, or from other field geological constraints (Table 2, Supplementary File 1). IRSL ages were calculated by dividing the D_E by the environmental dose rate for each sample. Dose rates were determined using ICP-MS techniques and include contribution from radioisotope concentrations and cosmic contribution in dilution from water content (Prescott and Hutton, 1994; Adamiec and Aitken, 1998; Aitken, 1998). IRSL ages are reported at 1-sigma standard error. Dose Rate information and age models for samples dated by IRSL are shown in Table 2 and Supplementary File 1.

Timing of terrace abandonment was established using depth profile and surface exposure dating using ^{10}Be isotopes from the quartz-rich terrace-capping sediments (e.g., Gosse and Phillips, 2001; Frankel et al., 2007; Hidy et al., 2010). Sampling strategy consisted of digging >2 m deep soil pits with a backhoe or by hand and collecting 30–100 pebble-size clasts at 30–50 cm depth intervals. Each sampling interval was confined to a ± 5 cm sampling horizon, except for pebbles collected directly on the surface. In localities of thin (<1m) terrace deposits, sampling was confined to the uppermost bedrock (sandstone) for surface exposure dating. Soil profiles were described, logged, and sampled for soil texture and LOI content at each site (Table 1). Samples were sent to the Lawrence Livermore National Lab (LLNL), PRIME Lab in Purdue University, or the Desert Research Institute (DRI) to be processed. Beryllium (Be) from the quartz fraction separated from the amalgamated clasts at each depth interval was extracted following similar methods given in Kohl and Nishiizumi (1992) and Licciardi (2000). An accelerator mass spectrometer measured the ^{10}Be isotopic concentrations. Following Be extraction procedures and isotopic concentrations measurements, a Monte Carlo approach in Matlab from Hidy et al., (2010) and CRONUS Age Calculator from Balco et al., (2008) provided the age models for each terrace depth profile and surface sample. This approach yielded abandonment surface ages that account for post-depositional exposure and erosion (Table 3; Supplemental File 2). Age models include measured density constraints of terrace deposits, which varies between 1.41–1.58 ± 0.05 g/cm^3 for upper soil horizons, 1.61–1.75 ± 0.05 g/cm^3 for mix of gravel and soil horizons, 1.82–1.89 ± 0.05 g/cm^3 for gravel layers, and 2.4 ± 0.2 g/cm^3 for bedrock sandstone beneath terrace strath. Local site production rates for each depth profile and surface sample are determined using revised spallogenic and muonogenic production rate calibrations of Heyman (2014) in the CRONUS

online calculator (Balco et al., 2008), scaled for topographic shielding, latitude, and elevation using the constant production-rate models of Lal (1991) and Stone (2000). Detailed sample information, AMS results, and age model parameters for TCN ^{10}Be geochronology are shown in Table 3 and Supplementary File 2.

The geomorphic significance of the IRSL and the TCN ^{10}Be depth profile are different. IRSL dating provides an age estimate of terrace-capping sediment deposition. Abandonment of a surface is revealed by models of a ^{10}Be depth profile or surface age (Anderson et al., 1996; or Repka et al., 1997). The combination of results from IRSL and TCN at the same site allow for independent, complementary assessment of the ages and provide brackets of the timing of terrace capping gravel deposition and subsequent abandonment.

TABLE 2. Feldspar IRSL and Quartz OSL Data and Ages for Corral Hollow and Lone Tree, San Joaquin County, California.

Sample	Location (Lat/Long)	Elv (m)	Depth (m)	% Water content[a]	K (%)[b]	U (ppm)[b]	Th (ppm)[b]	Total Dose (Gy/ka)[c]	Equivalent Dose (Gy)	n[d]	Scatter[e]	Age (yrs)[f]	Range (ka)	Geological unit
Corral Hollow Creek														
CH-IRSL-1	37.652647°N, 121.473613°E	204	5.3	3 (27)	2.37 ± 0.05	4.22 ± 0.22	15.9 ± 0.4	6.93 ± 0.13	-	-	-	-	>200-300 ka?	QP: Plio/Pleistocene
CH-IRSL-2	37.652647°N, 121.473613°E	204	5	4 (61)	1.61 ± 0.09	2.03 ± 0.2	6.23 ± 0.5	3.40 ± 0.16	-	-	-	-	>200-300 ka?	QP: Plio/Pleistocene
CH-IRSL-3	37.655844°N, 121.469072°E	157	8.0	0 (44)	1.62 ± 0.06	2.81 ± 0.20	8.96 ± 0.57	3.96 ± 0.16	377 ± 29	10 (14)	29%	**95,170 ± 8,290**	87 - 104	QP: Plio/Pleistocene
CH-IRSL-T9	37.655887°N, 121.469072°E	156.5	7.5	25 (33)	1.67 ± 0.04	1.96 ± 0.14	5.14 ± 0.35	4.33 ± 0.16	373 ± 36	6 (15)	37%	**86,130 ± 8,870**	77 - 95	T9 terrace
CH-OSL-T9	37.655887°N, 121.469072°E	156.5	7.5	25 (33)	1.67 ± 0.04	1.96 ± 0.14	5.14 ± 0.35	2.8 ± 0.11[g]	87 ± 7.2[g]	26 (28)	43%	31,450 ± 2,900[g]	29 - 34[g]	T9 terrace
CH-IRSL-T7	37.664328°N, 121.471036°E	110	4	2 (23)	1.67 ± 0.06	1.62 ± 0.27	5.25 ± 0.56	3.44 ± 0.21	175 ± 6.2	2 (15)	20%	**50,870 ± 3,580**	47 - 55	T7 terrace
Lone Tree Creek														
LTR-IRSL-T5-1	37.6121°N, 121.3793°E	119.3	2.7	0 (28)	1.48 ± 0.04	2.16 ± 0.18	5.46 ± 0.33	3.52 ± 0.13	45.6 ± 2.7	3 (20)	39%	**12,950 ± 900**	12 - 14	T5 terrace
LTR-IRSL-T5-2	37.6121°N, 121.3793°E	118.3	3.7	3 (13)	0.51 ± 0.04	0.53 ± 0.12	2.45 ± 0.34	1.31 ± 0.12	276 ± 7.0	2 (24)	28%	**210,700 ± 20,290**	190 - 231	QP: Plio/Pleistocene
LTR-IRSL-T5-3	37.6121°N, 121.3793°E	118.7	3.3	0 (21)	0.79 ± 0.03	1.08 ± 0.15	3.04 ± 0.21	1.95 ± 0.09	94.5 ± 2.3	5 (18)	42%	**31,090 ± 1,400**	30 - 32	T5 terrace
LTR-IRSL-T5-3[h]	37.6121°N, 121.3793°E	118.7	3.3	0 (21)	0.79 ± 0.03	1.08 ± 0.15	3.04 ± 0.21	1.95 ± 0.09	94.5 ± 2.3	5 (18)	42%	**25,230 ± 1,300[h]**	24 - 27	T5 terrace
LTR-IRSL-T6-145 cm	37.6127°N, 121.3806°E	129	1.45	10 (31)	1.59 ± 0.04	1.75 ± 0.19	7.46 ± 0.28	3.71 ± 0.10	418 ± 12	4 (15)	30%	**112,370 ± 4,530**	108 - 117	QP: Plio/Pleistocene
LTR-IRSL-T6-165 cm	37.6127°N, 121.3806°E	129	1.65	5 (45)	1.54 ± 0.02	1.46 ± 0.10	6.48 ± 0.14	3.27 ± 0.05	418 ± 16	2 (20)	12%	**127,830 ± 5,270**	123 - 133	QP: Plio/Pleistocene
LTR-IRSL-T6-190 cm	37.6127°N, 121.3806°E	129	1.9	4 (16)	1.05 ± 0.04	1.14 ± 0.15	4.78 ± 0.31	2.63 ± 0.11	357 ± 9.4	5 (15)	32%	**139,450 ± 6,940**	133 - 146	QP: Plio/Pleistocene
LTR-IRSL-T7-210 cm	37.6162°N, 121.3777°E	127	2.1	8 (17)	1.23 ± 0.04	1.80 ± 0.21	4.51 ± 0.25	3.04 ± 0.12	203 ± 11	3 (20)	22%	**99,510 ± 6,570**	93 - 106	QP: Plio/Pleistocene

[a]Field moisture, with figures in parentheses indicating the complete sample saturation %. Dose rates calculated using 50% of the saturated moisture (i.e. 5 (47) = 47 * 0.5 = 24).

[b]Analyses obtained using high-resolution gamma spectrometry (high purity Ge detector).

[c]Includes cosmic doses and attenuation with depth calculated using the methods of Prescott and Hutton (1994). Cosmic doses were between 0.07-0.03 Gy/ka.

[d]Number of replicated equivalent dose (D_E) estimates used to calculate the total D_E. Figures in parentheses indicate total number of measurements included in calculating the represented D_E and age using the minimum age model (MAM) or central age model (CAM) dependent on scatter or field geological constraints; analyzed via single aliquot regeneration on quartz or feldspar grains.

[e]Defined as "over-dispersion" of the D_E values. Values >30% are considered to be poorly bleached or mixed sediments.

[f]Dose rate, D_E, and age for fine-grained 250-63 micron sized **K-feldspar**, post IR230C; no fade observed. Exponential + linear fit used on D_E, errors to one sigma.

[g]Dose rate and age for fine-grained 250-63 micron sized **quartz**. Exponential + linear fit used on D_E, errors to one sigma. **Preferred ages shown in bold**.

[h]Dose rate and age for LTR-IRSL-T5-3 using a minimum age model (MAM) from a signle aliquot.

TABLE 3. Sample data information, AMS analytical results, and age models for terrestrial cosmogenic nuclide (TCN) ^{10}Be Geochronology

Sample	Location (Lat/Long)	Elv (m)	Depth (cm)[a]	Production Rate (atoms g^{-1} yr^{-1})		Shielding Factor[d]	Density (g/cm3)[e]	Quartz (g)	Be Carrier (mg)	^{10}Be/^{9}Be[f,g] (10^{-15})	Error ^{10}Be/^{9}Be[f,g] (10^{-15})	^{10}Be Conc. (atoms/g. quartz)[g,h,i]	Error ^{10}Be Conc. (atoms/g. quartz)[g,h,i]	Error ^{10}Be Conc. %	Model age (ka)[j]	Age range (ka)
				Spallation[b]	Muons[c]											
CH-T10Upper*	37.637586°N, 121.465457°E	333	90	6.245	0.233	0.999950	2.40	15.04	0.2525	327.81	4.21	393525.3235	5841.0700	1.48%	**113.5 ± 9.6**	**104 - 123**
CH-T10Lower-135cm	37.655190°N, 121.466815°E	184	135	6.245	0.233	0.999703	1.61	15.58	0.2542	356.15	3.30	415637.2098	2811.2679	1.43%		
CH-T10Lower-175cm	37.655190°N, 121.466815°E	184	175	6.245	0.233	0.999703	1.82	15.05	0.2534	234.67	2.49	282126.4171	2091.6495	2.00%		
CH-T10Lower-205cm	37.655190°N, 121.466815°E	184	205	6.245	0.233	0.999703	1.82	20.06	0.2531	218.75	2.39	196994.1102	2794.2326	1.62%		
CH-T10Lower-235cm	37.655190°N, 121.466815°E	184	235	6.245	0.233	0.999703	1.82	20.08	0.2533	160.43	2.16	144157.2356	2680.6717	2.30%		
															102.9 [+11.1, -8.8]	**94 - 114**
CH-T10Lower															314.3 [+26.7, -26.4]	288 - 341
CH-T7-50cm	37.664382°N, 121.471057°E	114	50	6.245	0.233	0.999557	1.75	19.28	0.2542	209.63	2.54	197225.3654	4948.9238	1.19%		
CH-T7-100cm	37.664382°N, 121.471057°E	114	100	6.245	0.233	0.999557	1.89	12.26	0.2526	71.91	1.32	104563.9810	3662.9788	1.30%		
CH-T7-150cm	37.664382°N, 121.471057°E	114	150	6.245	0.233	0.999557	1.89	14.14	0.2529	135.65	1.94	172586.0954	2610.9161	1.33%		
CH-T7-200cm	37.664382°N, 121.471057°E	114	200	6.245	0.233	0.999557	1.89	8.05	0.2245	59.91	1.29	116601.2269	2219.8413	1.54%		
															41.3 [+0, -1.1]	**40 - 41**
CH-T7															42.4 [+0, -9.7]	33 - 42
LTR-T5N-55cm	37.612137°N, 121.379257°E	122	55	6.245	0.233	0.999896	1.75	1.832	0.2520	19.54	1.60	175301.1194	14850.1076	8.47%		
LTR-T5N-85cm	37.612137°N, 121.379257°E	122	85	6.245	0.233	0.999896	1.89	4.111	0.2575	23.25	1.61	95350.5748	6797.3785	7.13%		
LTR-T5N-105cm	37.612137°N, 121.379257°E	122	105	6.245	0.233	0.999896	1.89	0.405	0.2521	2.632	0.71	89865.0434	30661.9303	34.12%		
LTR-T5N-175cm	37.612137°N, 121.379257°E	122	175	6.245	0.233	0.999896	1.89	1.095	0.2598	3.413	0.70	46641.3151	11602.8868	24.88%		
															33.9 [+13.7, -21.1]	**13 - 48**
LTR-T5N															40.0 [+13.2, -21.8]	16 - 60

*Sample collected for bedrock (sandstone) exposure age dating with an overlying 85cm of regolith/soil. All other samples collected in depth profiles at intervals of 30-40 cm from the surface to the bottom of the soil pit.

[a]Depth horizon includes sampling thickness of ±5 cm

[b]Constant (time invariant) local production rate based on Lal (1991) and Stone (2000). A sea level, high latitude value of 4.5 at ^{10}Be g-1 was used.

[c]Constant (time invariant) local production rate based on Heisinger et al. (2002a, 2002b).

[d]Geometric shielding correction using CRONUS online calculator

[e]Average density values measured from terrace samples composed of upper soil horizons (1.41 - 1.58 ± 0.05 g/cm3), mix of gravel and soil (1.61 - 1.75 ± 0.05 g/cm3), gravel layers (1.82 - 1.89 ± 0.05 g/cm3), and sandstone bedrock beneath strath (2.4 ± 0.2 g/cm3).

[f]Isotopes ratios were normalized to ^{10}Be standards prepared by Nishiizumi et al., (2007) with a value of 2.85×10^{12} and using a ^{10}Be half-life of $1.36 \times 10^{6} \pm 0.07$ years

[g]Uncertainties are reported at the 1σ confidence interval

[h]A mean chemistry blank value of ^{10}Be/^{9}Be = $1.4202 \times 10^{-15} \pm 1.8411 \times 10^{-16}$ was used to correct for background for samples CH-T10Upper, CH-T10Lower-TCN, and CH-T5-TCN. A mean chemistry blank value of 10Be/9Be = $0.4718 \times 10^{-15} \pm 0.2111 \times 10^{-15}$ was used to correct for background for samples LTR-T5N.

[i]Propagated uncertainties inlcude error in the blank, carrier mass (1%), and counting statistics

[j]Range of age models based from Hidy et al. (2010) Matlab depth profile simulator for depth profiles and Balco et al. (2008) CRONUS Age Calculator for bedrock surface exposures. **Preferred model ages shown in bold.**

Data reporting format following Frankel [2010].

Ages of Plio-Pleistocene units

The IRSL samples provide geochronological constraints for the uppermost tilted Plio-Pleistocene sediments (QP3). We sampled fine sand to silt-rich layers at multiple stratigraphic depths within QP3 in the Corral Hollow Creek below the strath of the T9 (Figs. 7c and 7d), and Lone Tree Creek below the T7, T6 and T5 straths (Fig. 9). Total stratigraphic thickness of QP3 varies from >60 m at Lone Tree Creek to 10–50 m at Corral Hollow Creek. An IRSL sample comes from a buff yellowish brown thin bedded silt-rich layers intercalated with calcic mudstone and poorly sorted gravels in a natural exposure of the uppermost QP3 strata below T9 strath contact south of Corral Hollow Creek (Figs. 7c–d and 10). The sample yielded an IRSL age of 95.2 ± 8.3 ka (Table 2). In uppermost stratigraphic levels of QP3 in Lone Tree Creek, an IRSL sample comes from >10 cm thick grey color fine sand to silt-rich layer collected beneath T7 strath contact (Figs. 9 and 10). The sample yielded an IRSL age of 99.5 ± 6.6 ka (Table 2). Down-section ~5m of QP3 in Lone Tree Creek, three IRSL samples comes from >50 cm thick gray color fine sand to silt-rich layer collected below T6 strath (Figs. 9 and 10). The three samples collected at 145 cm, 165 cm, and 195 cm depth in a soil pit yielded IRSL ages of 112.4 ± 4.5 ka, 127.8 ± 5.2 ka, and 139.4 ± 6.9 ka (Table 2), respectively. At the lowest stratigraphic levels and down-section ~10m of QP3 in Lone Tree Creek, exposed near the modern stream level, one IRSL sample comes from >30 cm thick brownish red fine grain to silt-rich layers intercalated with poorly sorted alluvial gravels collected below the T5 strath contact (Figs. 9 and 10). The sample yielded an IRSL age of 210.7 ± 20.3 ka (Table 2).

Terrace ages

IRSL and TCN ^{10}Be samples in terrace deposits were collected in Corral Hollow Creek and Lone Tree Creek to constrain timing of terrace formation and terrace abandonment.

Corral Creek

T10-Upper (BBF hanging wall)

A TCN ^{10}Be surface exposure sample was collected from a hand-dug soil pit in a surface south of Corral Hollow Creek interpreted to correlate to the highest T10 terrace located in the hanging wall of the BBF at 333 m elevation (CH-T10Upper; Fig. 2a). Site location did not permit for depth profile sampling from lack of sufficient deposit thickness and limited preservation of terrace gravels. Soil profile indicated a thin (0.90 cm) terrace stratigraphy of sandy soils horizons overlying a strongly petrocalcic sandstone bedrock strath (Table 1). These field observations may indicate T10 in the BBF hanging wall represents a pediment surface.

An uppermost bedrock sandstone sample was collected at the 90 ± 5cm depth below the inferred T10 strath contact. We used the CRONUS Age Calculator to provide a model surface exposure age of 113.5 ± 9.6 ka using the time-independent (St) scaling (Table 3; Supplementary File 2). The model age of ~113 ka accounts for 85cm of overlying soil and regolith cover. Alternative time-dependent (Lm) and nuclide-dependent (LSDn) scaling age models yielded similar results of 106.8 ± 8.6 ka and 117.4 ± 7.6 ka, respectively (Supplementary File 2).

T10-Lower (BBF footwall)

A backhoe-excavated soil pit in the T10 terrace located in the footwall of the BBF, correlated with the mapped T10 surface in the BBF hanging wall (Fig. 4), provided TCN ^{10}Be samples from a depth profile (CH-T10Lower; Fig. 8). Site selection for depth profile targeted the

highest accessible planar geomorphic surface of T10 in the BBF footwall, which forms a prominent well-exposed terrace thread on both the south and north sides of Corral Hollow Creek (Fig. 4). Soil profile characteristics include a thick upper clay-rich Bt horizon (0–125 cm) overlying alluvial gravels with well-developed pedogenic carbonate Bkt and Bk soils (12–250 cm). A disconformable contact at ~125 cm depth defines a sharp change in clay content, %carbonate, and lack preserved of upper terrace gravel stratigraphy (Fig. 8). These observations may imply as much as 125cm of post-abandonment soil inflation.

Four amalgamated gravel depth profile samples (135 cm, 175 cm, 205 cm, 235 cm) were used in our age model calculations. ^{10}Be concentration decreases with depth, which satisfies the Hidy et al., (2010) model assumption of constant inheritance with depth. We fit 10,000 Monte Carlo solutions to provide a preferred best-fit age of 102.9 [+11.1, -8.8] ka with 2 sigma confidence for terrace age abandonment (Fig. 8; Table 3). The best fit age of ~103 ka for T10 implies 125cm of soil inflation. All model input parameters are provided in Supplementary File 2. In contrast, if we model the T10 depth profile without observed soil inflation, the model age solutions indicate a best fit age of 314.3 [+26.7, -26.4] ka (Fig. 8; Table 3).

T9

A natural exposure south of Corral Hollow Creek provided a well-exposed outcrop of T9 terrace deposits for IRSL dating (Figs. 4 and 7c–d). A strath contact and angular unconformity differentiate the basal T9 gravels (elv. 157 m) from the underlying alluvial fan deposits of QP3 (Fig. 7c–d). Terrace deposits below the T9 surface (elv. ~165 m) consist of ~8 m thick multiple fining upward sequences of imbricated thick to very thick-bedded pebble to cobble size gravels, and locally medium bedded sand channel lenses. An IRSL sample was collected from a 20–30 cm thick lenticular coarse-grained sand layer, located 50 cm above the T9 strath contact with QP3 (Fig. 7c–d). The sample yielded an IRSL age of 86.1 ± 8.9 ka, which is in chronologic and stratigraphic order from the IRSL-dated older QP3 beneath the T9 strath contact (95.2 ± 8.3 ka; Table 2).

T7

A stream bank along Corral Hollow Creek exposed outcrops of T7 terrace gravels and overlying geomorphic surface sampled for both IRSL and a TCN ^{10}Be depth profile. A strath surface marks an angular unconformity between the basal T7 terrace gravels and the underlying older QP2 deposits (Figs. 7b and 8). Terrace stratigraphy is similar to T9, characterized by 3–8 m thick sequences of multiple 1–2m long lenticular sand-rich channel lenses intercalated with thick bedded pebble to cobble size gravel beds (Fig. 8). An IRSL collected in 10-15 cm thick medium to coarse grain fluvial channel sand layer in T7 deposits are located 4 m below T7 surface and 3–4 m above the strath overlying QP2 (Fig. 7b). The IRSL sample yielded an age of 50.9 ± 3.6 ka (Table 2), which is a maximum age bound for T7 surface abandonment given the stratigraphic position of the sample (Fig. 4).

A depth profile based on amalgamated-gravel samples from 50 cm, 100 cm, 150 cm, and 200 cm below the surface were used in our TCN ^{10}Be age model calculations. ^{10}Be concentration decreases with depth, but provides poor model fit to the profile. Samples at the 100 cm and 150 cm depths are interpreted as potential outliers and excluded in our age model calculation. This is consistent with field observations that these samples likely include sampling errors collected from a poorly exposed recessive escarpment of T7 (Fig. 8). We fit 100,000 Monte Carlo solutions to

provide a preferred best-fit age of 41.3 [+0, -1.1] ka with 2 sigma confidence for terrace age abandonment (Table 3). The best fit age of ~41 ka accounts for no significant post-abandonment soil modification on T7, as suggested by field observations and soil data (Figs. 7b and 8; Table 1). For comparison, a model age calculation that includes all depth profile samples yields a similar age of 42.3 [+0, -9.7] ka, but with large uncertainties of 10 sigma (Table 3; Supplementary File 2). All model input parameters are provided in Supplementary File 2. Our TCN ^{10}Be age results provide a minimum age for T7 with a surface abandonment exposure age of ~41 ka. This is consistent with our maximum age constraints of T7 from IRSL terrace deposits age of ~51 ka.

T10-Lone Tree Creek

In-situ TCN ^{10}Be age results are not yet available for many terraces sampled at Lone Tree Creek (T10, T9, T7, T6). Nonetheless, QP3 strata exposed below T7, T6, and T5 strath contacts provide age constraints on overlying and stratigraphically younger terraces. The uppermost dated QP3 strata have an IRSL age of 99.5 ± 6.6 ka that places a bound on the maximum age for the surface abandonment of T10. This age of ~100 ka for T10 in Lone Tree Creek overlaps with uncertainty with T10 age results of ~113 ka (CH-T10Upper) and ~103 ka (CH-T10Lower) collected at Corral Hollow Creek (Table 3).

T5-Lone Tree Creek

In Lone Tree Creek, two IRSL samples were collected within T5 terrace deposits from a stream cut exposure. Both samples are within localized channel sand layers intercalated down-section and up-section by thick bedded imbricated pebble to cobbles rich gravels. The T5 terrace deposit thickness ranges between 3.5 m and 4.5m. A sample collected at a 3.3 m depth below T5 surface is from a 15–20 cm thick, a ~3 m long laminated coarse sand lens (Fig. 9). At shallower depths in a layer 2.7 m to 2.4 m below T5 surface, a sample was retrieved from a 30–10 cm thick medium- to fine-grained sand and gravel rich layer within a 3–5 m long channel complex (cross-bedded, erosional scours, lag-deposits; Fig. 6). IRSL samples yield ages of 31.1 ± 1.4 ka and 12.9 ± 0.9 ka, for at the material sampled at 3.3 m and 2.7–2.4 m depths below T5 surface, respectively (Fig. 9; Table 2). The ~13 ka from the 2.4 – 2.7 m depth is interpreted as a maximum age for T5 surface abandonment. The ~31 ka age of the 3.3 m-deep sample may represent the age of an older terrace deposit because this sample exhibits large age scatter with an over-dispersion of 42%. A minimum age model (MAM) of 25.2 ± 1.3 ka from a single aliquot suggests a possible younger age result more consistent with the overlying ~13 ka age deposits in T5 (Table 2; Supplemental File 1).

TCN ^{10}Be depth profile samples (55 cm, 85 cm, 105 cm, 175 cm) collected from a soil pit in T5 constrain terrace surface abandonment age. ^{10}Be concentration decreases overall with depth, but large uncertainties and poor fit characterize the model. Although the profile did not a produce viable age model, excluding the sample at 55cm depth. Monte Carlo solutions yields a best fit age of 40.0 [+13.2, -21.8] ka with 2 sigma (Table 3; Supplemental File 2). Upper soil profile horizon (0-25cm) has evidence of disturbance from agricultural activity, which suggests ~25cm of soil inflation (Fig. 9). Monte Carlo solutions that include correction for soil inflation yield a best fit age of 33.9 [+13.7, -21.1] ka with 2 sigma (Table 3; Supplemental File 2), which overlaps with uncertainties to our IRSL age results of T5 (13-31 ka).

Age summary

Our IRSL and TCN ^{10}Be age data provide a consistent chronology of terrace formation and abandonment relative to the age model for older Plio-Pleistocene units (QP). Progressive unconformities and folding of QP1–QP3 indicate syntectonic deposition accompanied fault-related folding associated with the BBF and SJF along the eastern Diablo Range. Tilted and faulted lacustrine deposits in QP1 indicate the BBF has been active since at least middle Pleistocene time (600–800 ka), given correlation to the Corcoran Clay dated based on radiometric and paleomagnetic data of ash beds (Lettis 1982 and references therein). Progressive angular and buttress unconformities of QP2–QP3 indicate the BBF had sustained structural uplift through 211–100 ka from our IRSL data. IRSL age results from QP3 at Lone Tree Creek show ages are in chronologic and stratigraphic order from ~211 ka in QP3 basal strata exposed along the modern stream level; 139–112 ka for strata ~10 m up-section in QP3; and ~100 ka for strata ~5 m up-section in QP3 (Fig. 9; Table 2). Our age results from QP3 correlate well to other stratigraphic and paleontological data from bison fossils of Los Banos Alluvium (535 to 80 ka) recognized near Los Banos Reservoir, interpreted as regionally extensive deposits along the eastern the Diablo Range foothills (Lettis 1982; Unruh and Lettis, 1991).

IRSL and TCN ^{10}Be age results constrain terrace formation, surface abandonment, and incision for multiple terraces in Corral Hollow and Lone Tree. In Corral Hollow Creek, TCN ^{10}Be age data from footwall and hanging wall T10 terraces across the BBF range between 103 ka and 113 ka, respectively (Table 3). T10 correlates regionally along the eastern Diablo Range piedmont across both sites at Corral Hollow Creek and Lone Tree Creek. In Lone Tree Creek, IRSL age constraints from uppermost QP3 strata indicate overlying T10 terrace formation is no older than ~100 ka (Table 2), which overlaps with uncertainties in the T10 age results from Corral Hollow (103–113 ka). Age results of younger terraces (T9–T5) are consistent with incremental terrace formation and abandonment between ~86 ka and ~13 ka. T9 terrace deposits in Corral Hollow Creek are ~86 ka (Table 2). T7 in Corral Hollow brackets the timing of terrace deposition and surface abandonment to the interval between ~51 ka (IRSL) and ~41 ka (TCN ^{10}Be), respectively (Tables 2 and 3). Age results from the youngest dated terrace T5 in Lone Tree Creek indicate terrace deposition ranges between 13 and 31 ka, with ~13 ka representing the preferred age for uppermost terrace deposits (Table 2).

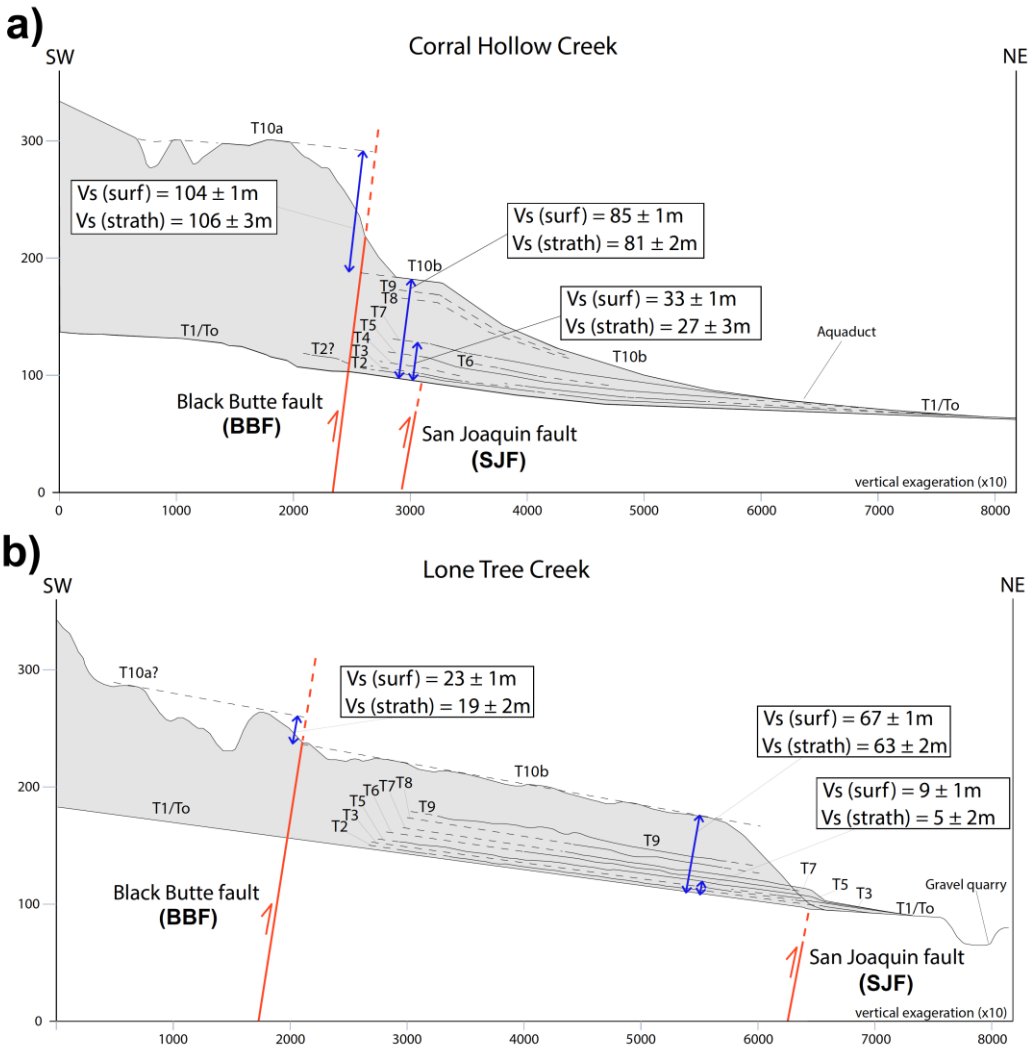

Figure 10. Vertical separation measurements (Vs) across the Black Butte fault and San Joaquin fault based on terrace and long river profiles data shown in Figure 6 for Corral Hollow Creek **(a)** and Lone Tree Creek **(b)**. The range of terrace surface Vs (surf) and terrace strath Vs (strath), including associated uncertainties are given in meters.

IMPLICATIONS FOR SEISMIC HAZARDS

Quaternary uplift and slip rates

Deformed and offset Pleistocene–Holocene strath terraces and progressive angular unconformities within the Plio-Pleistocene units (QP1–QP3) demonstrate that surface thrusting and fault-related folding persisted across both the Black Butte and San Joaquin faults throughout the late Quaternary. To estimate Black Butte fault slip, we use vertical separation between pairs of offset terraces (T10) to constrain uplift (Fig. 10). We use this uplift and fault dip to solve for shortening and fault slip, assuming reverse dip slip on the fault. To determine rates, we divide the amount of vertical separation, shortening, and fault slip by our age data (Table 4). For deformation by blind or fold-related faulting (San Joaquin fault), we use differential relief between terrace threads (T10, T9, T7, T5) and modern channels. Vertical separations for each strath terraces are plotted with our age data to constrain incision rates, assuming incision is result of fault-related

uplift (Fig. 11). Fault dip and structural models allow for the vertical component of deformation to be translated into fault slip rates (Table 4).

Black Butte fault

Offset surfaces and strath levels of T10 constrain the vertical offset across the Black Butte fault (BBF) since ~100 ka. In Corral Hollow Creek, T10 is elevated ~200 m above the modern channel and has a slope gradient of 0.6° in the hanging wall. T10 in the footwall is elevated ~100 m above the channel and has a slope gradient of 0.74°. We assign total range of fault vertical separation for T10 of 104 ± 1m (surface) and 106 ± 3m (strath) across the BBF (Fig. 10a). Offset measurements are based on topographic profiles north of Corral Hollow Creek because that location exhibits the most extensive and continuous exposure of the T10 surface (Figs. 2a–b, and 6a). Fault outcrops and hanging wall strata indicate the fault dips 40° (± 2) to the SW (Figs. 2–5). The fault truncates tilted Plio-Pleistocene (QP1–QP3) units and overlying T10 deposits in the footwall (Fig. 4). Rate calculations using a combined T10 age of 105.0 ± 18.1 ka yield an uplift rate of 1.03 ± 0.20 mm/yr and a fault slip rate of 1.63 ± 0.38 mm/yr across the BBF in Corral Hollow Creek (Table 4). All rates incorporate uncertainties in fault dip, age, vertical separation, and range of interpretation in using terrace surface and strath elevations for offset markers. Younger terraces are not well preserved in hanging wall of the BBF. A possible vertical separation of 6–9 m across T2 is suggested by projection of the terrace riser across the fault (Fig. 10a). The <13 ka of T3 implies that the fault slip rate of ~1 mm/yr has been sustained for the past 100 kyr. In Lone Tree Creek, a possible remnant T10 terrace or T10 pediment in the BBF hanging wall potentially correlates to T10 mapped in the footwall. If correct, the vertical separation from the terrace surface is 23 ± 1 m and 19 ± 2 for the terrace strath (Fig. 10b). Using the T10 age constraint from the Lone Tree Creek site of 99.5 ± 6.6 ka suggest both the uplift rate of 0.23 ± 0.03 mm/yr and fault slip rate of 0.41 ± 0.10 mm/yr are lower than at Corral Hollow Creek (Table 4).

San Joaquin fault

Vertical incision, tilting, and folding of strath terraces T10–T1 to east of the BBF attest to fault-related uplift of footwall fault splays associated with the blind SJF. We interpret the SJF as a 30–42°SW dipping blind thrust based on map relations, structural geometry of the BBF and SJF, and long wavelength terrace deformation pattern (Figs. 2, 4, 10). In Corral Hollow Creek, differential relief of strath terraces relative to the modern channel as measured from terrace profiles indicate vertical incision (uplift) of 85 ± 1 m and 81 ± 2 m for T10, and 33 ± 1 and 27 ± 3.0 m for T7 for terrace surface and strath levels, respectively (Fig. 10a). Linear regression of the age versus vertical separation (Vs) of T10 (105.0 ± 18.1 ka), T9 (86.1 ± 8,9 ka), and T7 (41–51 ka) terraces in Corral Hollow Creek, yields an average incision (uplift) rate of 0.81 ± 0.02 mm/yr and fault slip rate of 1.43 ± 0.24 mm/yr since ~100 ka (Fig. 11; Table 4). In Lone Tree Creek, topographic profiles of strath terraces T10–T1 in the SJF hanging wall demonstrates differential uplift relative to the modern channel. Vertical separation (Vs) of terrace surfaces and strath levels are 67 ± 1 and 63 ± 2 m for T10, and 9 ± 1 and 5 ± 2m for T5, respectively (Fig. 10b). Linear regression best fit of age-vertical separation is based on T10 (99.5 ± 6.6 ka) and T5 (12.95 ± 0.9 ka) (Fig. 11; Table 2). Rates calculations yield a long-term average incision rate (uplift) of 0.91 ± 0.23 mm/yr and a fault slip rate of 1.11 ± 0.20 mm/yr (Table 4). Using a ~100 ka age for T10 in Lone Tree Creek is maximum age bound translating into minimum deformation rates for San Joaquin fault, as the age constraint is from uppermost dated QP3 units underlying T10 terrace deposits.

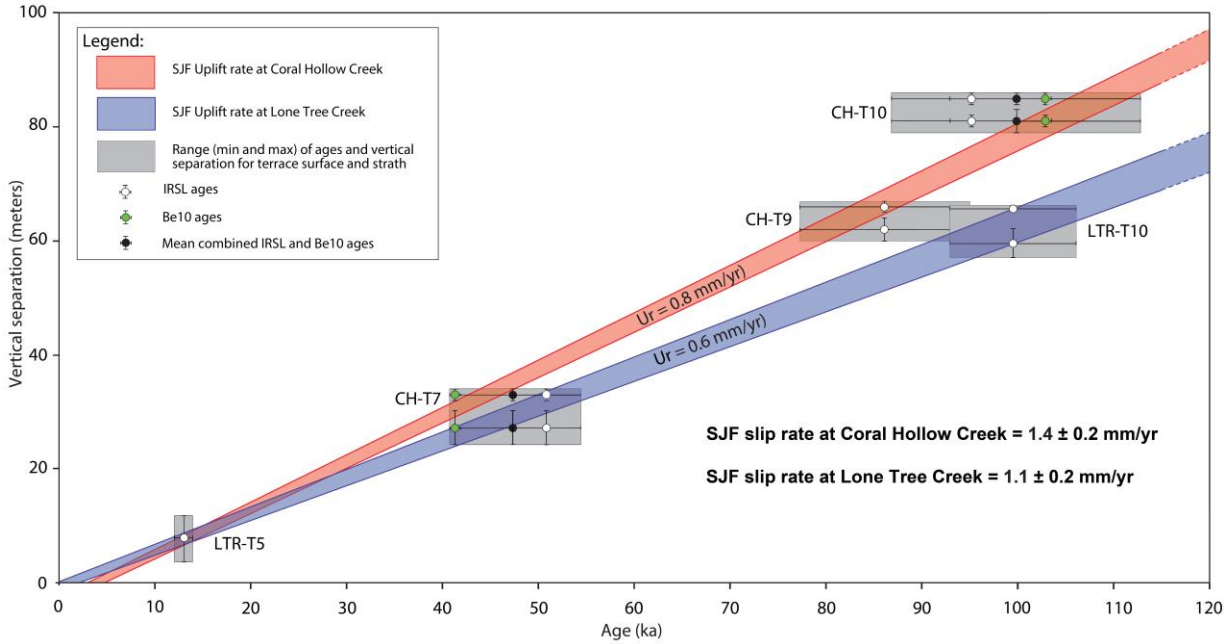

Figure 11. Vertical incision (uplift) rates (Ur) measurements shown as best-fit linear regression plots of vertical separation (meters) versus age (ka). Vertical separation (Vs) measurements are based on differential relief of terrace surface and terrace strath levels with the modern channel shown in Figure 10. Resulting fault slip rates are calculated based on 30–42° fault ramp for the San Joaquin fault (SJF). Age constraints of terraces are from IRSL and ^{10}Be age data (see Tables 2 and 3). Gray boxes indicate bounds of minimum and maximum terrace ages with range of vertical separation based on terrace surfaces to terrace strath levels.

TABLE 4. Uplift, shortening, and fault slip rates for the Black Butte fault (BBF) and San Joaquin fault (SJF).

	Vertical offset Terrace surf. (m)	Vertical offset Terrace strath (m)	Terrace Age (ka)	Fault dip (degrees)	Vertical sep. rate (mm/yr)	Shortening rate (mm/yr)	Fault slip rate (mm/yr)
BBF (Corral Hollow Creek)	104 ± 1	106 ± 3	105.0 ± 18.1	40 ± 2	1.03 ± 0.20	1.25 ± 0.32	1.63 ± 0.38
BBF (Lone Tree Creek) ?	23 ± 1m	19 ± 2	99.5 ± 6.6	36 ± 6	0.23 ± 0.03	0.34 ± 0.11	0.41 ± 0.10

	Fault dip (degrees)	Incision rate (mm/yr) Best-fit linear regression	Shortening rate (mm/yr)	Fault slip rate (mm/yr)
SJF (Corral Hollow Creek)	36 ± 6	0.81 ± 0.02	1.16 ± 0.28	1.43 ± 0.24
SJF (Lone Tree Creek)	36 ± 6	0.63 ± 0.02	0.91 ± 0.23	1.11 ± 0.20

Note: Measured values of vertical separation, fault dip, and range of ages for terrace surface and terrace strath levels. Using these parameters, we calculated vertical separation rates, incision rates, shortening rates, and fault slip rates with corresponding uncertainties, which are based on the range (maximum and minimum) in the rate calculation.

Slip rate summary for the Black Butte–San Joaquin fault system

Fault slip rate on the Black Butte fault is 1.3–2.0 mm/yr (1.63 ± 0.38) at Corral Hollow Creek where the vertical separation of T10 (104–106 m) is greater than it is along strike to the southeast. At Lone Tree Creek, the vertical separation of T10 is 23–19 m, which implies a lower fault slip rate of 0.41 ± 0.10 mm/yr. The discrepancy, between the two sites is potentially explained by slip not accounted for on other strands of the Black Butte fault (Fig. 2a). Fault slip rate on the

blind San Joaquin fault ranges from 1.43 ± 0.24 mm/yr in Corral Hollow Creek to 1.11 ± 0.20 mm/yr in Lone Tree Creek (Fig. 11). Summing rates across the deformation zone of the Black Butte–San Joaquin fault system yield a fault slip budget that range between 2.2–3.7 mm/yr since ~100 ka (Table 4). Evidence of surface folding since ~13 ka is restricted to the San Joaquin fault. A possible offset <13 ka terrace may suggest Holocene surface faulting on the BBF.

Comparison with earlier studies

Our data from dated Pliocene-Pleistocene units and terrace deposits provide evidence of faulting and folding since ~210 ka across the Black Butte–San Joaquin fault system. Plio-Pleistocene syntectonic growth strata (QP1–QP3) record thrust-related folding between 211–100 ka. Abandoned strath terraces T10–T5 constrain differential vertical separation and fault-related incision across the two faults system from ~110 to <13 ka. An angular conformity between Miocene and Cretaceous bedrock units indicates the faults are likely reactivated older structures (Figs. 3 and 4).

The slip rate we report for the San Joaquin fault is higher but compares favorably with a previous study (Sowers et al., 2000). A fault slip rate of 0.08–0.54 mm/yr for terraces across a fold scarp of the San Joaquin fault at Lone Tree Creek is based on terrace vertical separations and absolute age data for T7 (55–83 ka), T5 (29–47ka), and T3 (16–32ka) (Sowers et al., 2000; Fig. 2c). U-series and ^{14}C samples of pedogenic carbonate weathering rinds and an assumed 30–60° fault dip is the basis of the rate estimate. The lower slip rate largely reflects vertical separation restricted to terraces T7–T1 (Figs 6 and 10), and an alternative age model for the same terraces mapped in Lone Tree Creek we dated using IRSL and TCN ^{10}Be terrace ages from Corral Hollow Creek. Sowers et al. (2000) report that ^{14}C ages for T5 (18-19 ka) and T3 (~15 ka) were considered too young when compared to U-series dates on the same pedogenic carbonate rinds. If, however, the ^{14}C results are appropriate, the terrace ages would be closer to our IRSL age data for T5. One uncertainty noted by Sowers et al. (2000) is that U-series dating requires that assuming the system is closed and that clasts and their rinds are not recycled, and that the pedogenic carbonate weathering rind in not inherited nor record an earlier history of growth. Future age results from multiple TCN ^{10}Be depth profiles across T10, T9, T7, and T6 in Lone Tree and T5, T4, T3, and T2 in Corral Hollow will provide data to better understand the method-dependent age discrepancy.

Regional strain rates for southwestern Sacramento–San Joaquin Delta

Geodetic data indicate a 1.9–3.5 mm/yr shortening (convergence) rate and a 4.4–5.4 mm/yr dextral strike-slip rate along the western border of the San Joaquin Valley (Prescott et al., 2001; d'Alessio et al., 2005). A comparison of geodetic and geologic shortening rates reveals the percentage of the geodetic rate accounted for by slip on the fault system, and the degree of slip partitioning. Our geological shortening rates are 1.0–1.6 mm/yr for the BBF, and 0.7–1.4 mm/yr for the SJF (Table 4). A combined 1.7–3.0 mm/yr for the total shortening partitioned across the Black Butte–San Joaquin fault system broadly overlap with published geodetic convergence rates (1.9–3.5 mm/yr). Rate comparison at the Tracy–Livermore latitude indicate that most of the convergence is accounted on the BBF and SJF. Other range parallel faults at the same latitude in the Sacramento–San Joaquin Delta, such as the West Tracy and Vernalis Fauts may in turn absorb little convergence rates, thereby implying fault slip rates <<1 mm/yr on these reverse faults. Our study does not constrain whether the BBF or SJF accommodate the 4.4–5.4 mm/yr of dextral strike-slip rates indicated by geodetic data. However, the Midway fault to the NW or other range parallel strike-slip faults to the SE (Ortigalita fault) are likely candidates that absorb the dextral

strain for the eastern Diablo Range. A previous study on the West Tracy fault near the Clifton Court Forebay site, indicates long-term vertical separation rates <1 mm/yr based on structural relief of Miocene sediments in seismic data, and Holocene delta marsh deposits interpolated from log cores (Unruh and Hitchcock, 2015). Additional in-situ age data from offset surficial deposits are needed to constrain both reverse and strike-slip fault slip rates at intermediate to short timescales on the West Tracy fault and Midway fault. No slip rate estimates based on in-situ age data exist for the Midway fault. To the south where the Great Valley thrust system is represented by the Orestimba fault, Quinto, Laguna Secca, and Panoche faults, fault slip rates based on soil chronosequence datasets are estimated to range between 0.2 to 1.8 mm/yr (Anderson and Piety 2001).

Implications for earthquake potential

New understanding of the fault activity of the Black Butte and San Joaquin fault system provides constraints of the potential earthquake hazards to the Sacramento–San Joaquin Delta region. Fault geometries frame the size of the potential earthquake. Each individual segment of the Black Butte and San Joaquin faults are at minimum ~30 km-long. Along strike, the San Joaquin fault extends ~85 km to the southeast along the mountain front (Fig. 1). Empirical scaling relationships indicate that surface fault lengths of the Black Butte and San Joaquin faults could generate Mw 6.2–6.8 and Mw 7.2–7.3 reverse-fault earthquakes, respectively (Stirling et al., 2013). If simultaneous ruptures occurred on both faults, scaling relationships indicate the fault system could generate an earthquake of Mw >7.

Paleoseismic records on the Black Butte–San Joaquin fault system are unknown. We speculate the Black Butte–San Joaquin fault system is likely characterized by millennia-timescale earthquake recurrence interval based on a loading slip rate of ~1–2 mm/yr on each the BBF and SJF and the absence of historical earthquakes. Our NEHRP-funded study has identified paleoseismic trench sites on Black Butte fault with the goal of developing a Holocene paleoearthquake chronology.

An earthquake and associated ground shaking on the Black Butte-San Joaquin fault system could profoundly affect the greater Delta region including critical water infrastructure such as levee systems, canals, and pipelines. New paleoseismic and geophysical data are therefore needed to improve seismic source characterization of the Black Butte–San Joaquin fault system to better understand the hazard. Our results provide insights to reevaluate existing seismic source models for the Sacramento-San Joaquin Delta to include the Black Butte–San Joaquin fault system, that could produce ~85 km long fault rupture associated with fault splays and fault network of the Great Valley thrust system.

Acknowledgments. This material is based upon work supported by the U.S. Geological Survey under Grant No. G18AP00093 and received collaborative support from the U.S. Geological Survey Earthquake Science Center in the research activities of seismic hazards in the Sacramento–San Joaquin Delta. We would like to particularly thank Stephen DeLong, Alexandra Pickering, and Andrew Cyr that have collaborated in the field data collection and age analyses. We would like to thank Shannon Mahan at the USGS Luminescence Lab for processing the IRSL age results, Alan Hidy at the Lawrence Livermore National Lab, Marc Caffee at PRIME Lab, Brad Sion at Desert Research Institute for processing the Beryllium lab analytical results. We thank the field assistance from Wes Johns, Sally Keating, and Garret Huddleston.

References

Aitken, M.J., 1998, An Introduction to Optical Dating, the Dating of Quaternary Sediments by the Use of Photon- Stimulated Luminescence: Oxford, UK, Oxford University Press, 267 p.

Amos, C.B., Burbank, D.W., Nobes, D.C., and Read, S.A.L., 2007, Geomorphic constraints on listric thrust faulting: Implications for active deformation in the Mackenzie Basin, South Island, New Zealand: Journal of Geophysical Research, v. 112, p. 1-24.

Anderson, R.S., Repka, J.L., and Dick, G.S., 1996, Explicit treatment of inheritance in dating depositional surfaces using in situ 10Be and 26Al: Geology, v. 24, p. 47-51.

Anderson, L.W. and Piety, L.A., 2001, Geologic seismic source characterization of the San Luis-O'Neill area, eastern Diablo Range, California for B.F. Sisk and O'Neill Forebay dams, San Luis Unit, Central Valley Project, California, U.S. Bureau of Reclamation, Seismotectonic Report 2001-2, 76 p.

d'Alessio, M.A., Johanson, I.A., Bürgmann, R, Schmidt, D.A., and M.H. Murray, 2005, Slicing up the San Francisco Bay Area: Block kinematics and fault slip rates from GPS-derived surface velocities. Journal of Geophysical Research 110, doi:10.1029/2004JB003496.

Dawson, T.E., 2013, Appendix A—Updates to the California Reference Fault Parameter Database—Uniform California Earthquake Rupture Forecast, Version 3 Fault Models 3.1 and 3.2 in Field, E. H. and others, 2013, Uniform California earthquake rupture forecast, version 3 (UCERF3)—The time-independent model: U.S. Geological Survey Open-File Report 2013–1165, 97 p., California Geological Survey Special Report 228, and Southern California Earthquake Center Publication 1792, http://pubs.usgs.gov/of/2013/1165/.

Dawson, T.E. and Weldon, R.J., 2013, Appendix B—Geologic-Slip-Rate Data and Geologic Deformation Model in Field, E. H and others, 2013, Uniform California earthquake rupture forecast, version 3 (UCERF3)—The time-independent model: U.S. Geological Survey Open-File Report 2013–1165, 97 p., California Geological Survey Special Report 228, and Southern California Earthquake Center Publication 1792, http://pubs.usgs.gov/of/2013/1165/.

Dibblee, T.W., Jr., 1981a, Preliminary geologic map of the Lone Tree Creek quadrangle, San Joaquin and Stanislaus Counties, California: United States Geological Survey Open-File Report 81-466, scale 1:24,000.

Dibblee, T.W., Jr., 1981b, Preliminary geologic map of the Tracy quadrangle, San Joaquin County, California: United States Geological Survey Open-File Report 81-464, scale 1:24,000.

Ducea, M., House, M.A., and Kidder, S., 2003, Late Cenozoic denudation and uplift rates in the Santa Lucia Mountains, California, Geology, v. 31, no. 2, p. 139-142.

Ellis, M.A. and Densmore, A.L., 2006, First-order topography over blind thrusts, in Willet, S.D., Hovius, N., Brandon, M.T., and Fisher, D.M., eds., Tectonics, Climate and Landscape Evolution, Volume 398: Boulder, Geological Society of America, p. 251-266.

Erslev, E.A., 1991, Trishear fault-propagation folding: Geology, v. 19, p. 617-620.

Field, E.H., Biasi, G.P., Bird, P., Dawson, T.E., Felzer, K.R., Jackson, D.D., Johnson, K.M., Jordan, T.H., Madden, C., Michael, A.J., Milner, K.R., Page, M.T., Parsons, T., Powers, P.M., Shaw, B.E., Thatcher, W.R., Weldon, R.J., II, and Zeng, Y., 2013, Uniform California earthquake rupture forecast, version 3 (UCERF3)—The time-independent model: U.S. Geological Survey Open-File Report 2013–1165, 97 p., California Geological

Survey Special Report 228, and Southern California Earthquake Center Publication 1792, http://pubs.usgs.gov/of/2013/1165/.

Gosse, J.C. and Phillips, F.M., 2001,F Terrestrial in situ cosmogenic nuclides: theory and application: Quaternary Science Reviews, v. 20, p. 1475-1560.

Guzofski, C.A., Shaw, J.H., Lin, G., and Shearer, P.M., 2007, Seismically active wedge structure beneath the Coalinga anticline, San Joaquin basin, California, J. Geophys. Res., 112, B03S05, doi:10.1029/2006JB004465.

Hancock, G.S., Anderson, R.S., Chadwick, O.A., and Finkel, R.C., 1999, Dating fluvial terraces with (super 10) Be and (super 26) Al profiles; application to the Wind River, Wyoming: Geomorphology, v. 27, p. 41-60.

Hardy, S. and Poblet, J., 1994, Geometric and numerical model of progressive limb rotation in detachment folds: Geology, v. v. 22, p. 371-374.

Jachens, R.C., Griscom, A., and C.W. Roberts. 1995. Regional extent of Great Valley basement west of the Great Valley, California: Implications for extensive tectonic wedging in the California Coast Ranges. Journal of Geophysical Research v. 100, no. B7, p. 12,769-12,790. July 10, 1995.

Jennings, C.W., 1994, Fault activity map of California and adjacent areas: California Department of Conservation, Division of Mines and Geology, Geologic Data Map No. 6, scale 1:750,000.

Jennings, C.W. and Bryant, W.A., 2010, Fault activity map of California: California Geological Survey Geologic Data Map No. 6.

Keller, E.A., Zepeda, R.L., Rockwell, T. K., Ku, T.L., and Dinklage, W.S., 1998, Active tectonics at Wheeler Ridge, southern San Joaquin Valley, California. Geological Society of America Bulletin v. 110, p. 298-310.

Krug, E.H., Cherven, V.B., Hatten, C.W., and Roth, J.C., 1992, Subsurface structure in the Montezuma Hills, southwestern Sacramento basin, in Cherven, V.B., and Edmondson, W.F., eds., Structural Geology of the Sacramento Basin: Volume MP-41, Annual Meeting, Pacific Section, Society of Economic Paleontologists and Mineralogists, p. 41-60.

Lettis, W.R., 1982, Late Cenozoic stratigraphy of the western margin of the central San Joaquin Valley, California: U.S. Geological Survey Open-File Repot 82-526, 203 p., scale 1:24,000.

Lettis, W. R., Wells, D. L., and Baldwin, J. N., 1997, Empirical observations regarding reverse earthquakes, blind thrust faults, and Quaternary deformation: Are blind thrust faults truly blind?: Bulletin of the Seismological Society of America, v. 87, no. 5, p. 1171-1198.

Mueller, K., and Suppe, J., 1997, Growth of Wheeler Ridge anticline, California: Implications for short-term folding behavior during earthquakes. Journal of Structural Geology, v. 19, p. 383-396.

Noller, J.S., Sowers, J.M., and Lettis, W.R., 1993, Quaternary geology of the Solyo and LoneTree Creek 7.5 minute quadrangles, California: U.S. Geological Survey Open File Report 93 224.

Page, M.T., Field, E. H., Milner, K.R., and Powers, P.M, 2013, Appendix N—Grand Inversion Implementation and Testing in Field, E. H and others, 2013, Uniform California earthquake rupture forecast, version 3 (UCERF3)—The time-independent model: U.S. Geological Survey Open-File Report 2013–1165, 97 p., California Geological Survey Special Report 228, and Southern California Earthquake Center Publication 1792, http://pubs.usgs.gov/of/2013/1165/.

Prescott, W.H., Savage, J.C., Svarc, J.L., and Manaker, D., 2001, Deformation across the Pacific-North American plate boundary near San Francisco, California: Journal of Geophysical Research, v. 106, no. B4, p. 6673-6682.

Repka, J.L., Anderson, R.S., and Finkel, R.C., 1997, Cosmogenic dating of fluvial terraces, Fremont River, Utah: Earth and Planetary Science Letters, v. 152, p. 59-73.

Rockwell, T.K., Keller, E.A., and Dembroff, G.R., 1988, Quaternary rate of folding of the Ventura Avenue anticline, western Transverse Ranges, southern California: Geological Society of America Bulletin, v. 100, no. 6, p. 850-858.

Rittenour, T.M., 2008, Luminescence dating of fluvial deposits: Applications to geomorphic, palaeoseismic and archaeological research: Boreas, v. 37, p. 613–635, doi:10.1111/j.1502-3885.2008.00056.x.

Rhodes, E.J., 2011, Optically stimulated luminescence dating of sediments over the past 200,000 years: Annual Review of Earth and Planetary Sciences, v. 39, p. 461– 488, doi:10.1146/annurev-earth-040610-133425.

Simoes, M., Avouac, J.-P., Chen, Y.-G., Sighvi, A.K., Wang, C.-Y., Jaiswal, M., Chan, Y.-C., and Bernard, S., 2007, Kinematic analysis of the Pakuashan fault tip fold, west central Taiwan: Shortening rate and age of folding inception: Journal of Geophysical Research, v. 112, p. 1-30.

Sowers, J.M., Noller, J.S., and Lettis, W.R., 1993, Quaternary geology of the Tracy and Midway 7.5

Sowers, J. M., Simpson, G. D., Lettis, W. R., and Randolph, C. E., 1998, Monoclinal folding of fluvial terraces along the San Joaquin fault near Tracy, California: U.S. Geological Survey, National Earthquake Reduction Program Final Technical Report, Award No. 1434-HQ-97-GR-03011.

Sowers, J.M., Sharp, W. D., Southard, R. J., and Ludwig, K. R., 2000, Quaternary deformation along East Front of the Diablo Range near Tracy, CA: U. S. Geological Survey, National Earthquake Hazards Reduction Program, Final Technical Report 99-HQ-GR-0101.

Sterling, R., 1992, Intersection of the Stockton and Vernalis faults, southern Sacramento Valley, California, in Chervon, V.B., and Edmondson, W.F., eds, Structural Geology of the Sacramento Basin: American Association of Petroleum Geologists Miscellaneous Publication 41, Pacific Section, p. 143-151.

Lettis, W.R., and Unruh, J.R., 1991, Quaternary geology of the Great Valley, California: in Morrison, R.B., ed., Quaternary non-glacial geology of the conterminous United States: Boulder, Colorado, Geological Society of America, Decade of North American Geology, v. K2.

Unruh, J., Sowers, J., Noller, J., and Lettis, W., 1992, Tectonic wedging and late Cenozoic evolution of the eastern Diablo Range mountain front, northwestern San Joaquin Valley, California, in Erskine, M.C., Unruh, J., Lettis, W.R., and Bartow, J.A., eds., Field Guide to the Tectonics of the Boundary Between the California Coast Ranges and Great Valley of California: Pacific Section, American Association of Petroleum Geologists, guidebook GB-70, p. 13-22.

Unruh, J.R. and Sawyer, T.L., 1995, Late Cenozoic growth of the Mt. Diablo fold and thrust belt, central Contra Costa County, California, and implications for transpressional deformation of the northern Diablo Range [abs.]: American Association of Petroleum Geologists, 1995 Pacific Section Convention Abstracts, 47 p.

Unruh, J.R. and Sundermann, S., 2006, Digital compilation of thrust and reverse fault data for the Northern California Map Database: Collaborative research with William Lettis & Associates, Inc., and the U.S. Geologic Survey: Final Technical Report submitted to the U.S. Geological Survey, National Hazards Reduction Program, Award No. 05- HQ-GR-0054, 20 p.

Unruh, J.R and Krug, K., 2007, Assessment and Documentation of Transpressional Structures, Northeastern Diablo Range, for the Quaternary Fault Map Database: Collaborative Research with William Lettis & Associates, Inc., and the U.S. Geological Survey: U. S. Geological Survey National Earthquake Hazards Reduction Program Award Number, Final Technical Report - 06HQGR0139.

Unruh, J.R. and Hitchcock, C.S., 2015, Detailed Mapping and Analysis of Fold Deformation Above the West Tracy Fault, Southern San Joaquin-Sacramento Delta, Northern California: Collaborative Research with Lettis Consultants International and InfraTerra: U. S. Geological Survey National Earthquake Hazards Reduction Program Award Number, Final Technical Report – G14AP00069

Wakabayashi, J. and Unruh, J. R., 1995, Tectonic wedging, blueschist metamorphism, and exposure of blueschists: Are they compatible? Geology, v. 23, no. 1, p. 85-88.

Wells, D. L. and Coppersmith, K. J., 1994, New empirical relationships among magnitude, rupture length, rupture width, rupture area, and surface displacement: Bulletin of the Seismological Society of America, v. 84, no. 4, p. 974-1002.

Wentworth, C.M., Blake, M.C.Jr., Jones, D. L., Walter, A.W., and Zoback, M.D. 1984. Tectonic wedging associated with emplacement of the Franciscan assemblage, California Coast Ranges. In Blake, M.C., ed., Franciscan geology of northern California. Pacific Section, Society of Economic Paleontologists and Mineralogists, Field Trip Guidebook 43, p. 163-173.

Wong, I.G., Ely, R.W., and Kollman, A.C., 1988, Contemporary seismicity and block tectonics of the Northern California and central Coast Range-Sierran Block boundary zone, California: Journal of Geophysical Research, v. 93, p. 7813-7833.

Wright, R.H., Hamilton, D.H., Hunt, T.D., Traubenik, M.L., and Shlemon, R.J., 1982, Character and activity of the Greenville structural trend, in Hart, E.W., Hirschfeld, S.E., and Schulz, S.S., eds., Proceedings, Conference on Earthquake Hazards in the Eastern San Francisco Bay Area: California Division of Mines and Geology Special Publication 62, p. 187-196.

Supplemental File 1. Dose rate information and age models for samples dated by infrared stimulated luminescence (IRSL) and optically stimulated luminescence (OSL) geochronology.

CH-IRSL-3: Age of deposition for IRSL on 250-63 µ feldspar grains using single aliquot analyses

Radial plot of all equivalent dose values (showing population clusters)

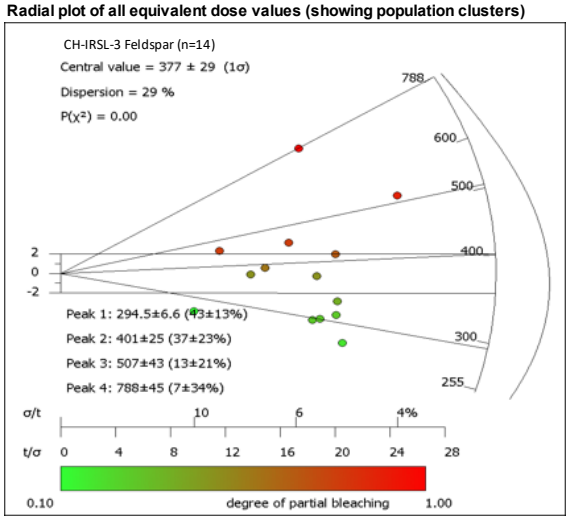

Radial plot of all equivalent dose values (showing lowest (youngest) population cluster)

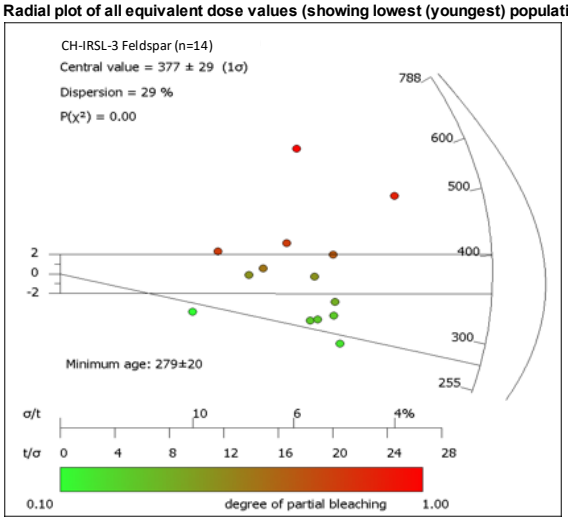

Probability plot from Riseo Analyst Program

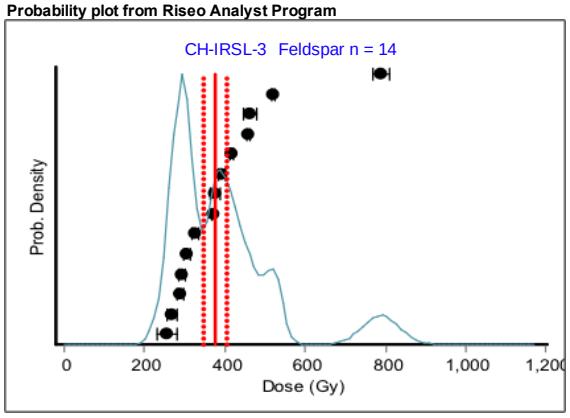

Equivalent Dose Models (No fading adjustment)
CAM: 377 ± 29 Gy (95,170 ± 8,290 years)
MAM: 279 ± 20 Gy (70,430 ± 5,820 years)
Weighted Mean: 343 ± 10.6 Gy (86,520 ± 4,440 years)
CAM = Central Age Model
MAM = Minimum Age Model
Galbraith, R.F., 2010, On plotting OSL equivalent doses. Ancient TL, V. 29, n1.
Graph generated from RadialPlotter-2017.jar
http://radialplotter.london-geochron.com
Version 8.13

CH-IRSL-4: Age of deposition for IRSL on 250-90 µ feldspar grains using single aliquot analyses

Radial plot of all equivalent dose values (showing population clusters)

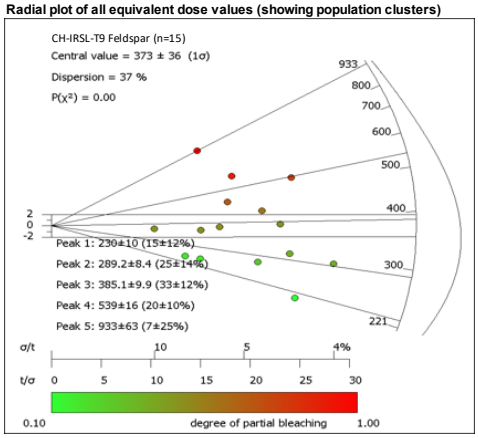

Radial plot of all equivalent dose values (showing lowest (youngest) population cluster)

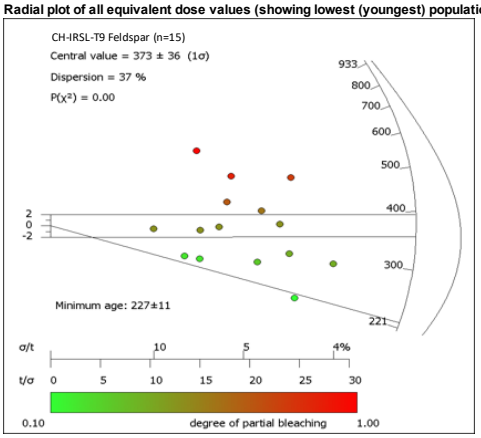

Probability plot from Riseo Analyst Program

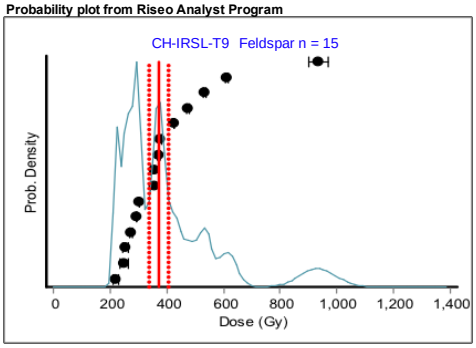

Equivalent Dose Models (No fading adjustment)
CAM: 373 ± 36 Gy (86,130 ± 8,870 years)
MAM: 227 ± 11 Gy (52,410 ± 3,160 years)
Weighted Mean: 310 ± 8.5 Gy (71,670 ± 3,240 years)
CAM = Central Age Model
MAM = Minimum Age Model
Galbraith, R.F., 2010, On plotting OSL
equivalent doses. Ancient TL, V. 29, n1.
Graph generated from RadialPlotter-2017.jar
http://radialplotter.london-geochron.com
Version 8.13

CH-South-OSL-4: Age of deposition for OSL on 250-63 µ quartz grains using single aliquot analyses

Radial plot of all equivalent dose values (showing population clusters)

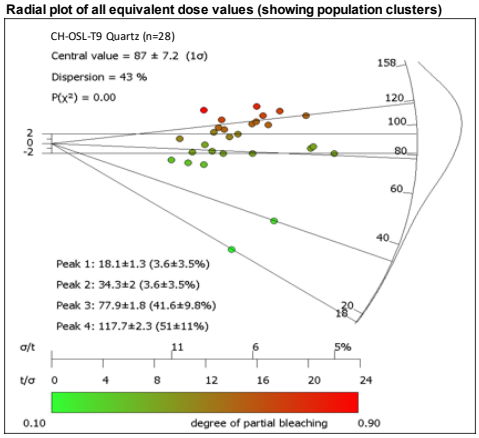

Radial plot of all equivalent dose values (showing lowest (youngest) population cluster)

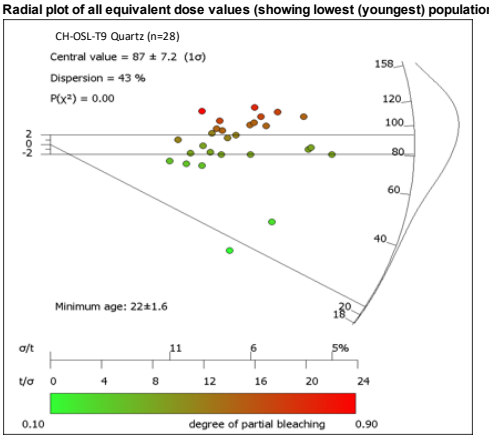

Probability plot from Riseo Analyst Program

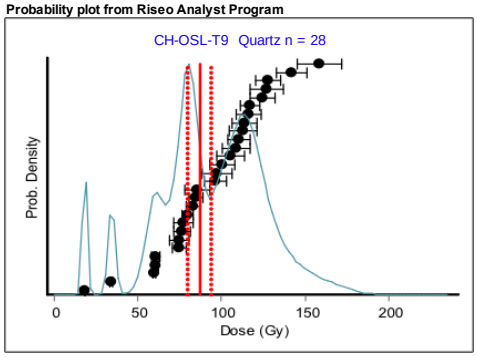

Equivalent Dose Models (No fading adjustment)
CAM: 87 ± 7.2 Gy (31,450 ± 2,900 years)
MAM: 22 ± 1.6 Gy (7,860 ± 660 years)
Weighted Mean: 52.7 ± 1.6 Gy (18,820 ± 960 years)
CAM = Central Age Model
MAM = Minimum Age Model
Galbraith, R.F., 2010, On plotting OSL
equivalent doses. Ancient TL, V. 29, n1.
Graph generated from RadialPlotter-2017.jar
http://radialplotter.london-geochron.com
Version 8.13

CH-IRSL-T7: Age of deposition for IRSL on 150-90 µ feldspar grains using single aliquot analyses

Radial plot of all equivalent dose values (showing population clusters)

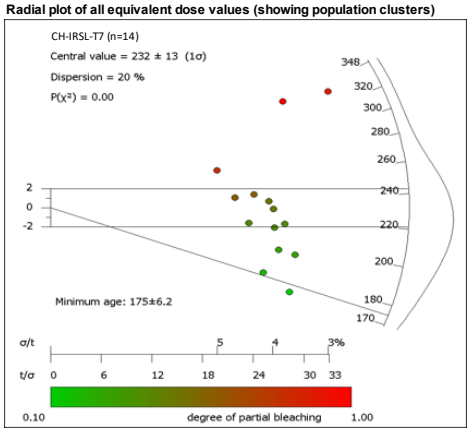

Radial plot of all equivalent dose values (showing lowest (youngest) population cluster)

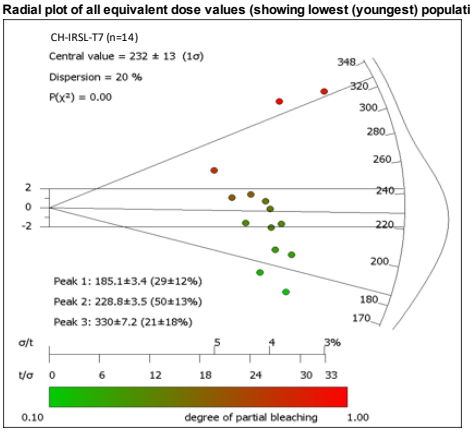

Probability plot from Riseo Analyst Program

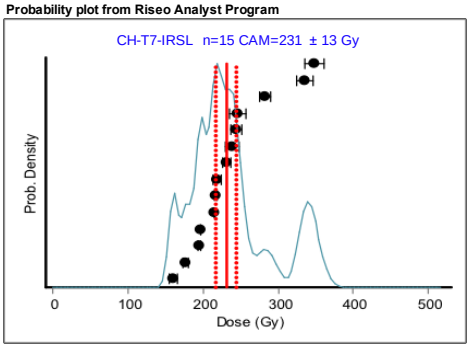

Equivalent Dose Models (No fading adjustment)
MAM: 175 ± 6.2 Gy (50,870 ± 3,580 years)
CAM: 232 ± 13 Gy (67,440 ± 5,580 years)
Weighted Mean: 208 ± 4.8 Gy (60,340 ± 3,930 years)
MAM = Minimum Age Model
CAM = Central Age Model
Galbraith, R.F., 2010, On plotting OSL equivalent doses. Ancient TL, V. 29, n1.
Graph generated from RadialPlotter-2017.jar
http://radialplotter.london-geochron.com
Version 8.13

LTR-IRSL-T5-1: Age of deposition for IRSL on 125-90 µ feldspar grains using single aliquot analyses

Radial plot of all equivalent dose values (showing population clusters)

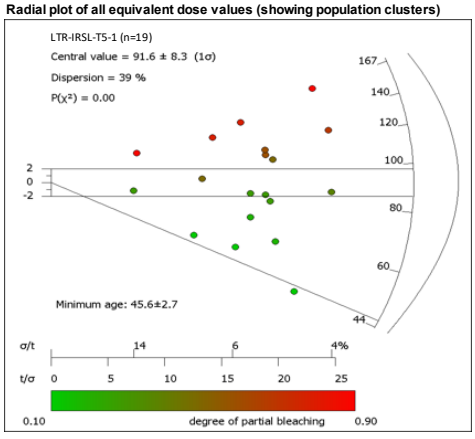

Radial plot of all equivalent dose values (showing lowest (youngest) population cluster)

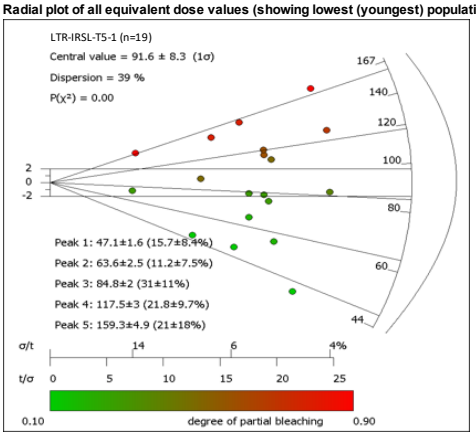

Probability plot from Riseo Analyst Program

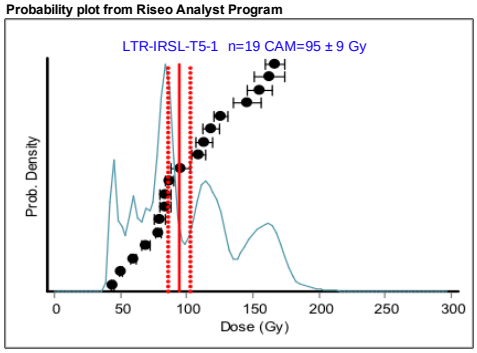

Equivalent Dose Models (No fading adjustment)
MAM: 45.6 ± 2.7 Gy (12,950 ± 900 years)
CAM: 91.6 ± 8.3 Gy (26,020 ± 2,550 years)
Weighted Mean: 72.8 ± 2.00 Gy (20,690 ± 940 years)
MAM = Minimum Age Model
CAM = Central Age Model
Galbraith, R.F., 2010, On plotting OSL equivalent doses. Ancient TL, V. 29, n1.
Graph generated from RadialPlotter-2017.jar
http://radialplotter.london-geochron.com
Version 8.13

LTR-IRSL-T5-2: Age of deposition for IRSL on 180-125 µ feldspar grains using single aliquot analyses

Radial plot of all equivalent dose values (showing population clusters)

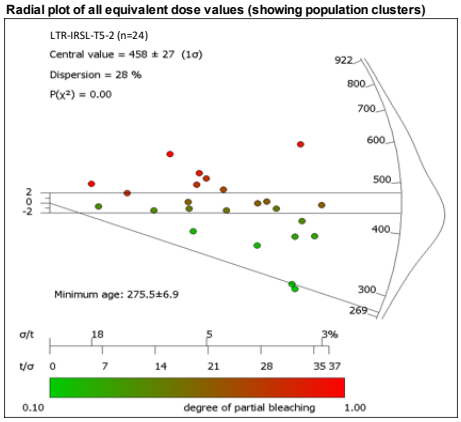

Radial plot of all equivalent dose values (showing lowest (youngest) population cluster)

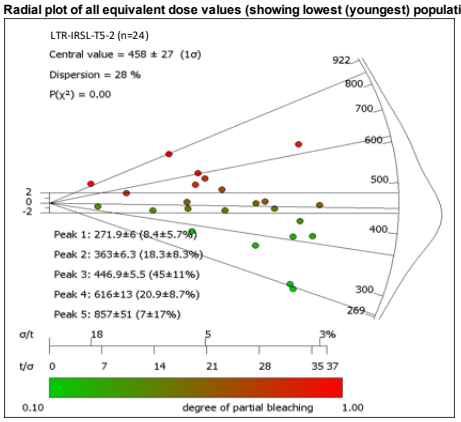

Probability plot from Riseo Analyst Program

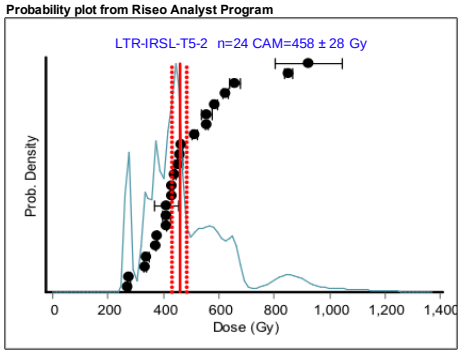

Equivalent Dose Models (No fading adjustment)
MAM: 276 ± 7 Gy (210,700 ± 20,290 years)
CAM: 458 ± 27 Gy (349,600 ± 38,510 years)
Weighted Mean: 382 ± 6.49 Gy (291,400 ± 27,550 years)
MAM = Minimum Age Model
CAM = Central Age Model
Galbraith, R.F., 2010, On plotting OSL
equivalent doses. Ancient TL, V. 29, n1.
Graph generated from RadialPlotter-2017.jar
http://radialplotter.london-geochron.com
Version 8.13

LTR-IRSL-T5-3: Age of deposition for IRSL on 250-63 µ feldspar grains using single aliquot analyses

Radial plot of all equivalent dose values (showing population clusters)

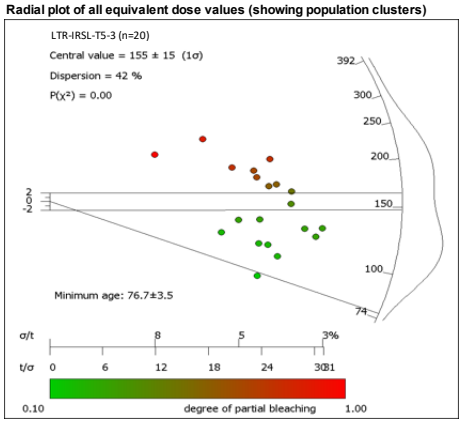

Radial plot of all equivalent dose values (showing lowest (youngest) population cluster)

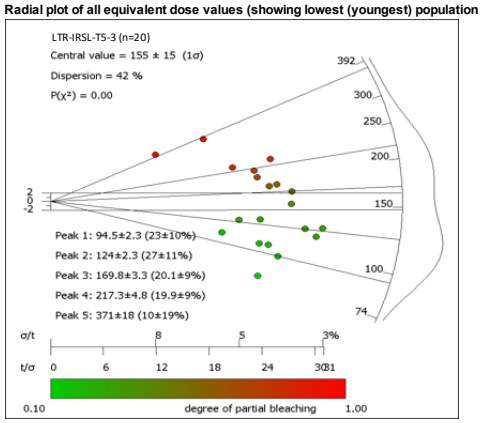

Probability plot from Riseo Analyst Program

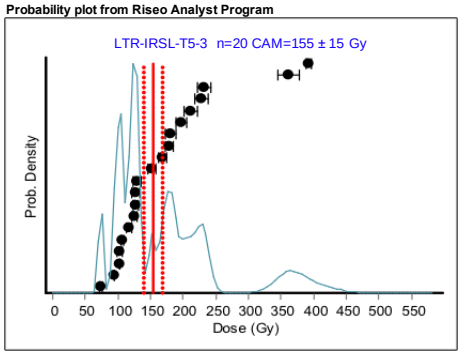

Equivalent Dose Models (No fading adjustment)
MAM/Peak 1: 94.5 ± 2.3 Gy (31,090 ± 1,400 years)
MAM (single aliquot): 76.7 ± 3.5 Gy (25,230± 1,300 years)
CAM: 155 ± 15 Gy (50,990 ± 5,450 years)
Weighted Mean: 122 ± 2.45 Gy (40,150 ± 1,720 years)
MAM = Minimum Age Model
CAM = Central Age Model
Galbraith, R.F., 2010, On plotting OSL
equivalent doses. Ancient TL, V. 29, n1.
Graph generated from RadialPlotter-2017.jar
http://radialplotter.london-geochron.com
Version 8.13

LTR-IRSL-T6-145 cm: Age of deposition for IRSL on 180-150 µ feldspar grains using single aliquot analyses

Radial plot of all equivalent dose values (showing population clusters)

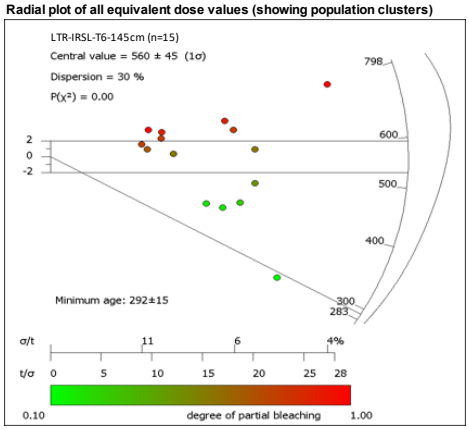

Radial plot of all equivalent dose values (showing lowest (youngest) population cluster)

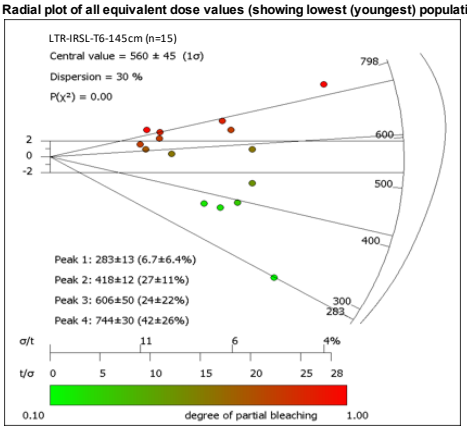

Probability plot from Riseo Analyst Program

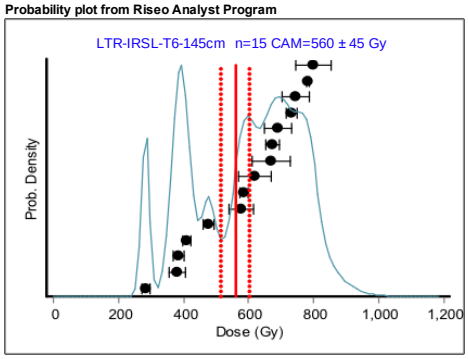

Equivalent Dose Models (No fading adjustment)
MAM: 292 ± 15 Gy (78,490 ± 4,570 years) anchored by 1 aliquot
CAM: 560 ± 45 Gy (150,540 ± 12,760 years)
PEAK 2: 418 ± 12 Gy (112,370 ± 4,530 years)
Weighted Mean: 523 ± 17.8 Gy (140,550 ± 6,200 years)
MAM = Minimum Age Model
CAM = Central Age Model
Galbraith, R.F., 2010, On plotting OSL
equivalent doses. Ancient TL, V. 29, n1.
Graph generated from RadialPlotter-2017.jar
http://radialplotter.london-geochron.com
Version 8.13

LTR-IRSL-T6-165 cm: Age of deposition for IRSL on 250-180 µ feldspar grains using single aliquot analyses

Radial plot of all equivalent dose values (showing population clusters)

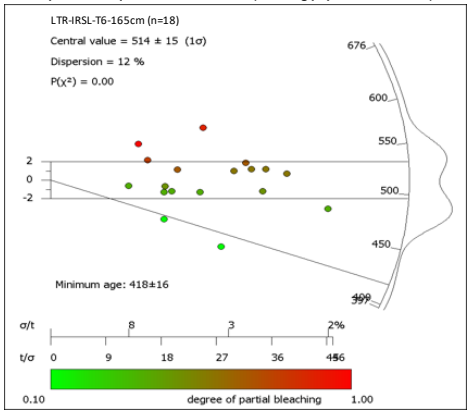

Radial plot of all equivalent dose values (showing lowest (youngest) population cluster)

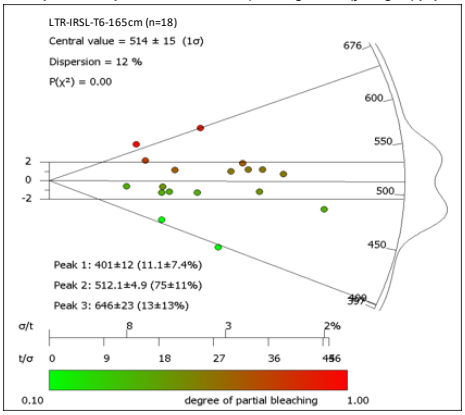

Equivalent Dose Models (No fading adjustment)
MAM: 418 ± 16 Gy (127,830 ± 5,270 years)
CAM: 514 ± 15 Gy (157,190 ± 5,210 years)
Weighted Mean: 501 ± 8.72 Gy (153,340 ± 3,620 years)
MAM = Minimum Age Model
CAM = Central Age Model
Galbraith, R.F., 2010, On plotting OSL
equivalent doses. Ancient TL, V. 29, n1.
Graph generated from RadialPlotter-2017.jar
http://radialplotter.london-geochron.com
Version 8.13

LTR-IRSL-T6-190 cm: Age of deposition for IRSL on 250-180 µ feldspar grains using single aliquot analyses

Radial plot of all equivalent dose values (showing population clusters)

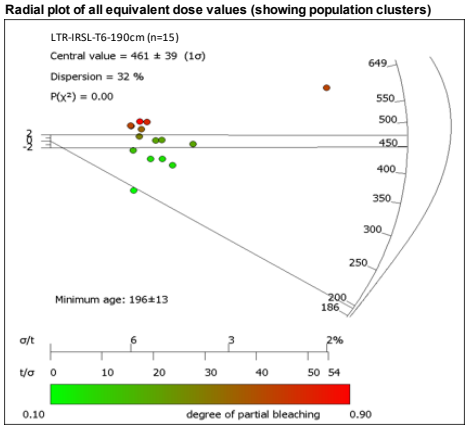

Radial plot of all equivalent dose values (showing lowest (youngest) population cluster)

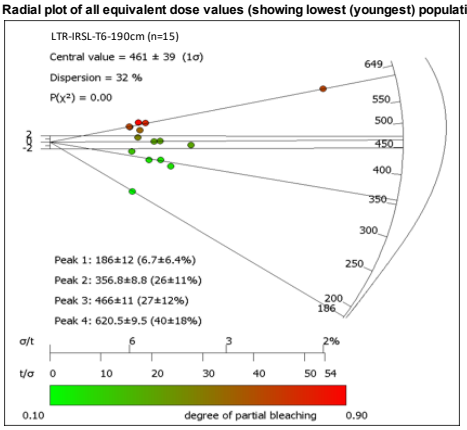

Probability plot from Riseo Analyst Program

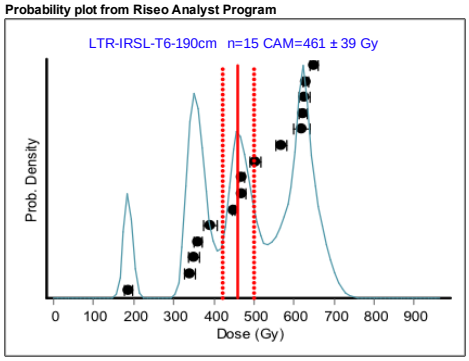

Equivalent Dose Models (No fading adjustment)
MAM: 196 ± 13 Gy (76,560 ± 6,030 years)
CAM: 461 ± 39 Gy (180,080 ± 17,150 years)
PEAK 2: 357 ± 9 Gy (139,450 ± 6,940 years)
Weighted Mean: 474 ± 11 Gy (185,190 ± 9,030 years)
MAM = Minimum Age Model
CAM = Central Age Model
Galbraith, R.F., 2010, On plotting OSL
equivalent doses. Ancient TL, V. 29, n1.
Graph generated from RadialPlotter-2017.jar
http://radialplotter.london-geochron.com
Version 8.13

LTR-IRSL-T7-210cm: Age of deposition for IRSL on 180-150 µ feldspar grains using single aliquot analyses

Radial plot of all equivalent dose values (showing population clusters)

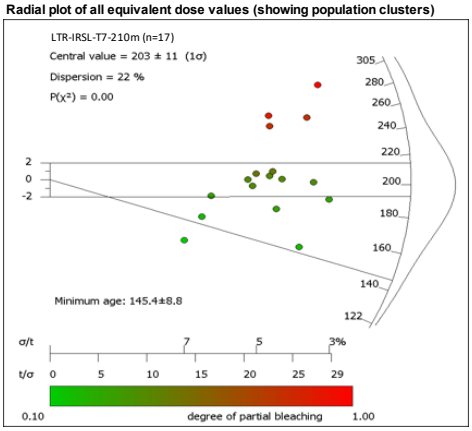

Radial plot of all equivalent dose values (showing lowest (youngest) population cluster)

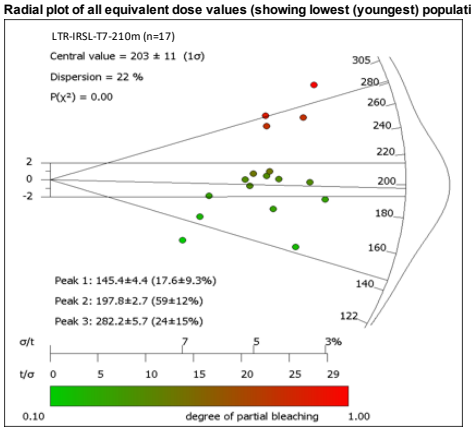

Probability plot from Riseo Analyst Program

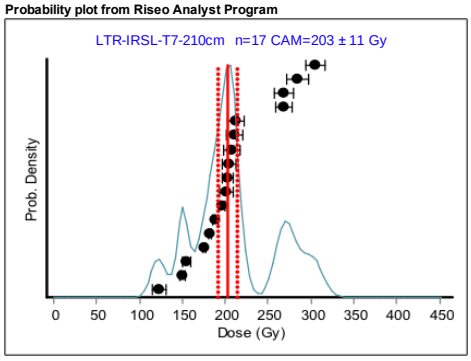

Equivalent Dose Models (No fading adjustment)
CAM: 203 ± 11 Gy (99,510 ± 6,570 years)
MAM: 145 ± 8.8 Gy (71,080 ± 5,110 years)
Weighted Mean: 196 ± 4.25 Gy (96,130 ± 4,210 years)
CAM = Central Age Model
MAM = Minimum Age Model
Galbraith, R.F., 2010, On plotting OSL
equivalent doses. Ancient TL, V. 29, n1.
Graph generated from RadialPlotter-2017.jar
http://radialplotter.london-geochron.com
Version 8.13

Supplemental File 2. Model parameters and data input for modeling terrestrial cosmogenic nuclide (TCN) Be10 surface exposure dating using CRONUS Age Calculator from Balco et al. (2008) and Depth Profile Simulator from Hidy et al. (2000).

CH-T10Upper: Be10 exposure dating of an erosional pediment surface into CH-T10Upper bedrock strath with 85 cm of regolith/soil cover.

CRONUS Age Calculator - Data input

Sample	Lat	Long	Elv (m)	Elv/Pressure handling flag	Sample thickness (cm)[a]	Sample density (g/cm3)[b]	Shield Correction[c]	Eorsion rates (cm/yr)[d]	Date sample collection
CH-T10Upper	37.637586	-121.46546	333	std	95	1.51	0.999950	0.00005	2018

Sample	Isotope	Mineral	Be10 Conc.	Error	Standard
CH-T10Upper	Be-10	quartz	393525.3235	5841.0700	KNSTD

[a]Sample thickness represents the total amount of material modelled for Be10 exposure dating that includes overlying 85cm of regolith/soil cover and 10 cm of bedrock (sandstone) sampled interval.

[b]Weighted average density measured from combined regolith/soil cover (85 cm @ 1.41 ± 0.05 g/cm3) and bedrock sandstone sample (10cm @ 2.4 ± 0.2 g/cm3).

[c]Geometric shielding correction using CRONUS online calculator

[d]Erosion rates derived from model constraints of neighboring CH-T10Lower using Hidy et al. (2010) Matlab depth profile simulator.

CRONUS Age Calculator- Age model results

Sample	Nuclide	St			Lm			LSDn		
		Age (yr)	Internal error (yr)	External error (yr)	Age (yr)	Internal error (yr)	External error (yr)	Age (yr)	Internal error (yr)	External error (yr)
CH-T10Upper	Be-10 (qtz)	113507	1781	9646	106827	1671	8606	117422	1846	7567

St: Time-independent scaling age model by Stone et al. (2000), which is based on Lal (1991).

Lm: Time-dependent scaling age model by Lal/Stone that accounts for geomagnetic field variations.

LSDn: Nuclide-dependent scaling age model by Lifton-Stato-Dunai.

Age results generated by CRONUS-Earth online calculators, Blaco et al. (2008).
https://hess.ess.washington.edu/
version 3

CH-T10Lower: Be10 depth profile dating of surface CH-T10Lower - Age model corrected for 125cm of soil inflation.

Model parameters and age results using Depth Profile Simulator from Hidy et al. (2000).

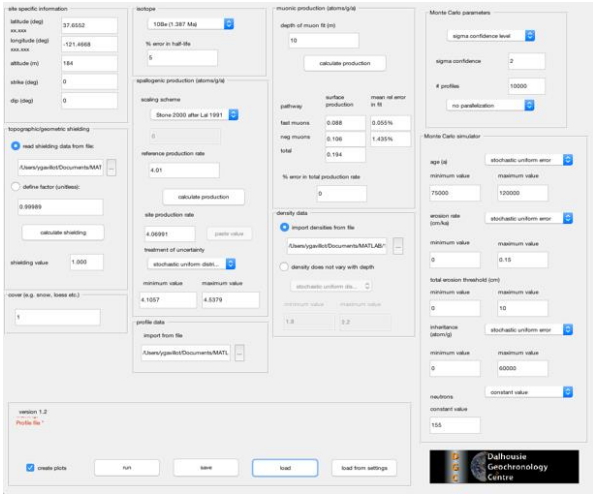

CH-T10lower (125 cm corrected for soil inflation; 2 sigma level; 10,000 runs)

	age (ka)	inheritance (10^4 atoms g^-1)	erosion rate (cm ka^-1)
mean	104.2	2.11	0.05
median	104.1	2.12	0.05
mode	103.2	2.16	0.06
min chi^2	107.0	2.02	0.01
maximum	119.9	4.75	0.10
minimum	88.9	0.00	0.00
Bayesian most probable	**102.9**	**2.29**	**0.05**
Bayesian 2-sigma upper	114.0	3.48	0.09
Bayesian 2-sigma lower	94.1	0.52	NaN

CH-T10Lower model plots - Age model corrected for 125cm soil inflation

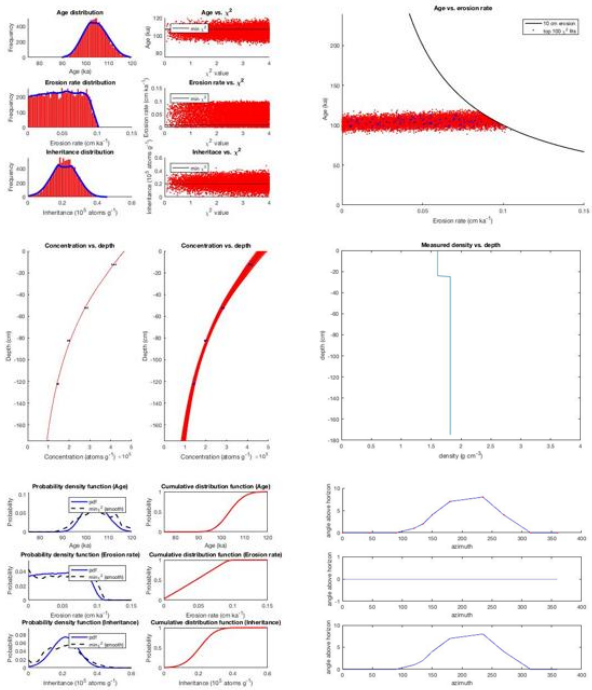

Model parameters and age results using Depth Profile Simulator from Hidy et al. (2000).

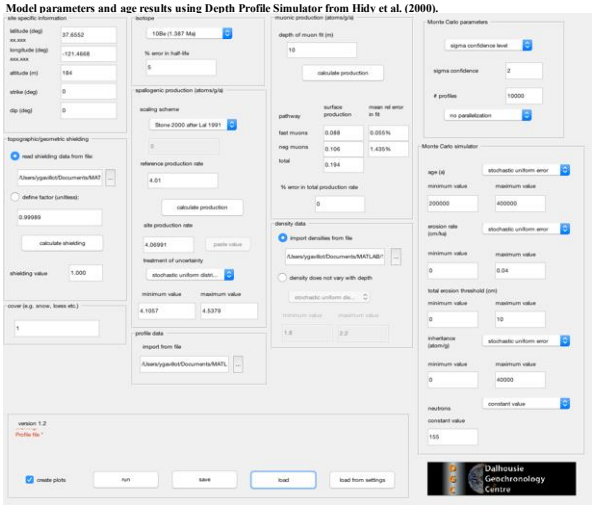

CH-T10Lower model plots - Uncorrected for soil inflation

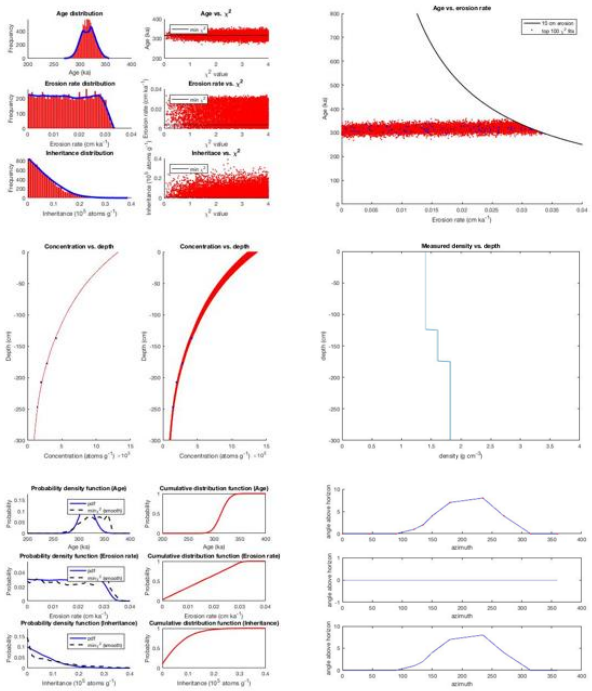

CH-T10lower (uncorrected; 2 sigma confidence level; 10,000 runs)

	age (ka)	inheritance (10^4 atoms g^-1)	erosion rate (cm ka^-1)
mean	316.3	0.66	0.02
median	316.2	0.53	0.02
mode	315.8	0.04	0.01
min chi^2	316.7	0.01	0.00
maximum	358.9	3.90	0.03
minimum	267.6	0.00	0.00
Bayesian most probable	**314.3**	**0.00**	**0.02**
Bayesian 2-sigma upper	341.0	2.07	0.03
Bayesian 2-sigma lower	287.6	NaN	NaN

CH-T7: Be10 depth profile dating of surface CH-T7 - Depth intervals 100cm and 150 cm excluded in model.

Model parameters and age results using Depth Profile Simulator from Hidy et al. (2000).

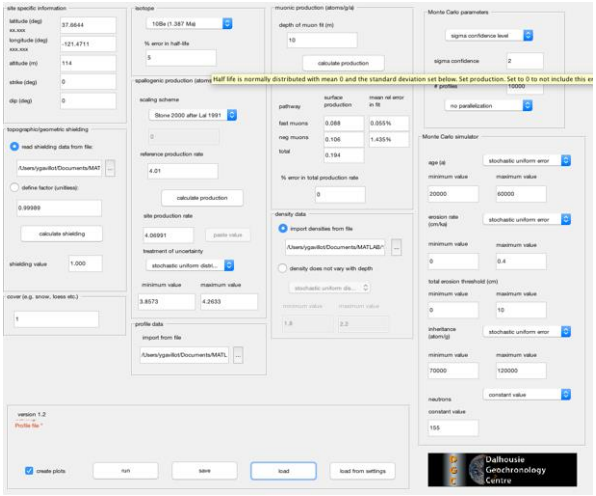

CH-T7 model plots - Depth intervals 100cm and 150 cm excluded in model.

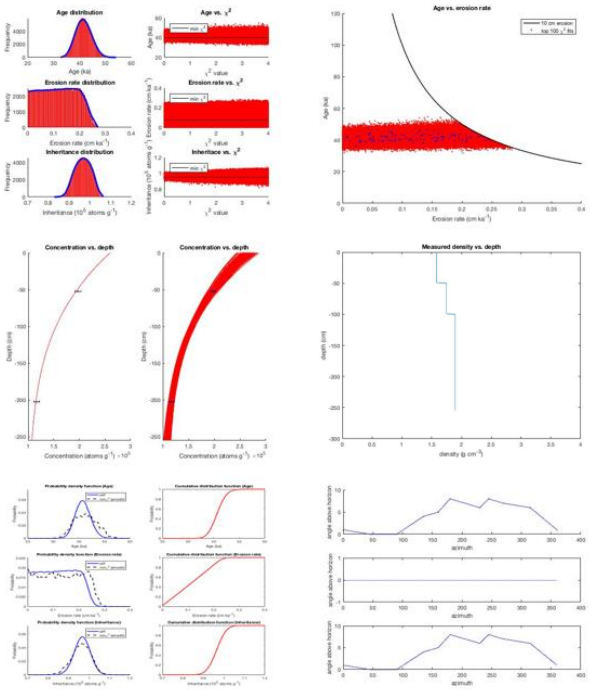

CH-T7 (100-150cm samples excluded in model; 2 sigma confidence level; 100,000 runs)

	age (ka)	inheritance (10^4 atoms g^-1)	erosion rate (cm ka^-1)
mean	36.8	12.49	0.15
median	30.5	12.50	0.12
mode	19.7	13.36	0.04
min chi^2	41.4	10.96	0.18
maximum	100.0	15.00	0.40
minimum	0.0	10.00	0.00
Bayesian most probable	**41.3**	**10.98**	**0.18**
Bayesian 2-sigma upper	41.3	10.98	0.18
Bayesian 2-sigma lower	40.2	10.93	0.17

CH-T7: Be10 depth profile dating of surface CH-T7 - All depth intervals included in model.

Model parameters and age results using Depth Profile Simulator from Hidy et al. (2000).

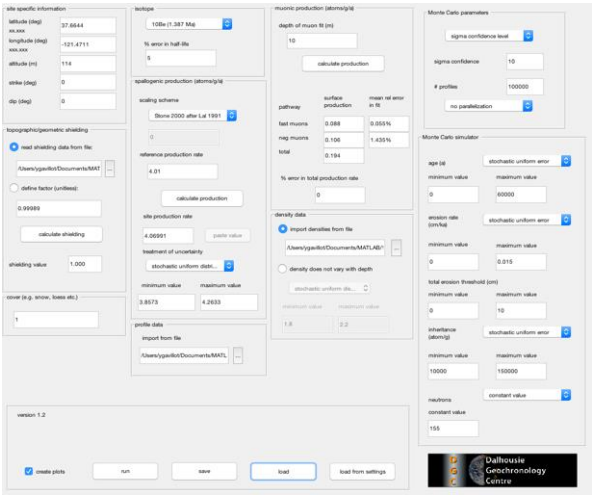

CH-T7 (all samples included in model; 10 sigma confidence level; 100,000 runs)

	age (ka)	inheritance (10^4 atoms g^-1)	erosion rate (cm ka^-1)
mean	30.0	8.00	0.01
median	30.0	7.99	0.01
mode	49.6	8.63	0.01
min chi^2	42.7	9.53	0.00
maximum	60.0	15.00	0.01
minimum	0.0	1.00	0.00
Bayesian most probable	**42.4**	**9.52**	**0.00**
Bayesian 2-sigma upper	42.4	9.52	0.00
Bayesian 2-sigma lower	32.7	9.24	0.00

CH-T7 model plots - All depth intervals included in model.

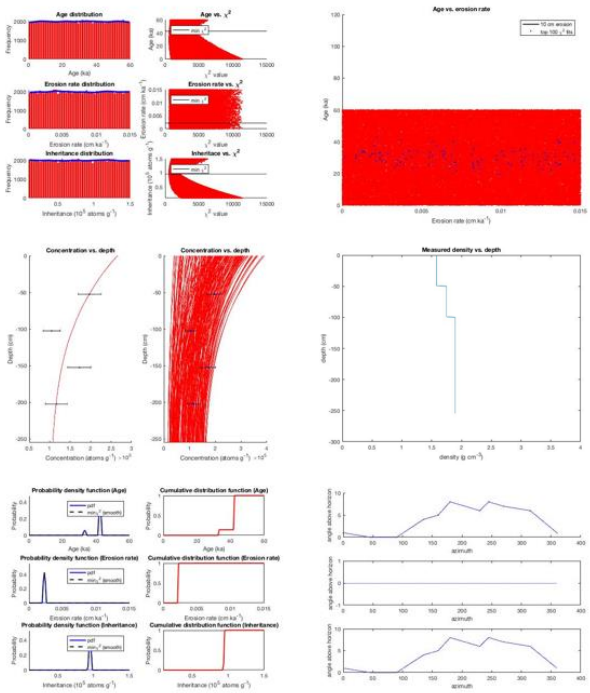

LTR-T5N: Be10 depth profile dating of surface LTR-T5N - Depth interval 55cm excluded in model.

Model parameters and age results using Depth Profile Simulator from Hidy et al. (2000).

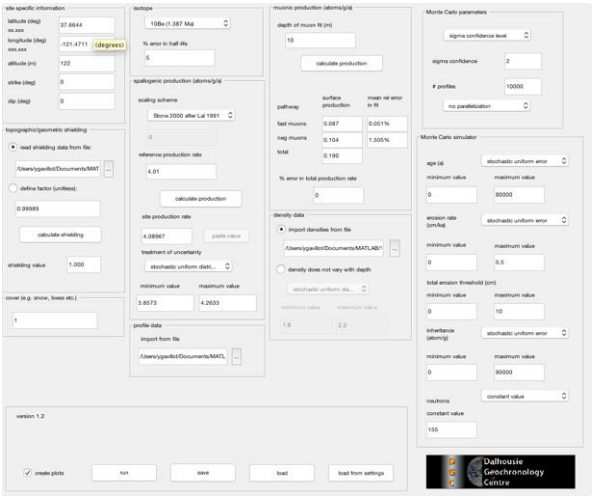

LTR-T5 (55 cm sample excluded in model; 2 sigma level; 10,000 runs)

	age (ka)	inheritance (10^4 atoms g^-1)	erosion rate (cm ka^-1)
mean	40.2	2.79	0.13
median	39.7	2.85	0.13
mode	31.2	1.88	0.14
min chi^2	53.1	1.13	0.17
maximum	72.8	5.67	0.46
minimum	19.9	0.00	0.00
Bayesian most probable	41.9	2.36	0.08
Bayesian 2-sigma upper	60.3	6.12	0.36
Bayesian 2-sigma lower	15.5	0.02	NaN

LTR-T5N model plots - Depth interval 55cm excluded in model

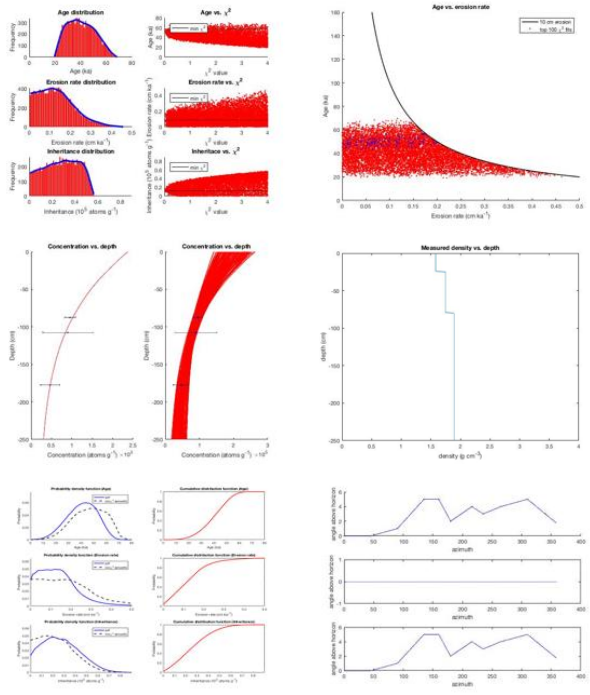

LTR-T5N: Be10 depth profile dating of surface LTR-T5N - Age model corrected for possible 25 cm soil inflation

Model parameters and age results using Depth Profile Simulator from Hidy et al. (2000).

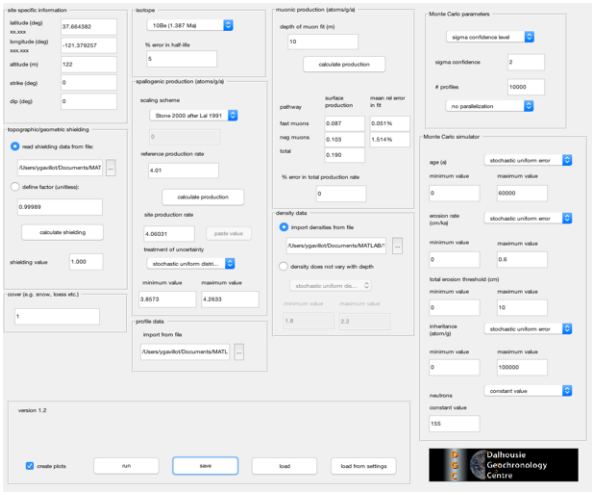

LTR-T5N model plots - Age model corrected for possible 25 cm soil inflation

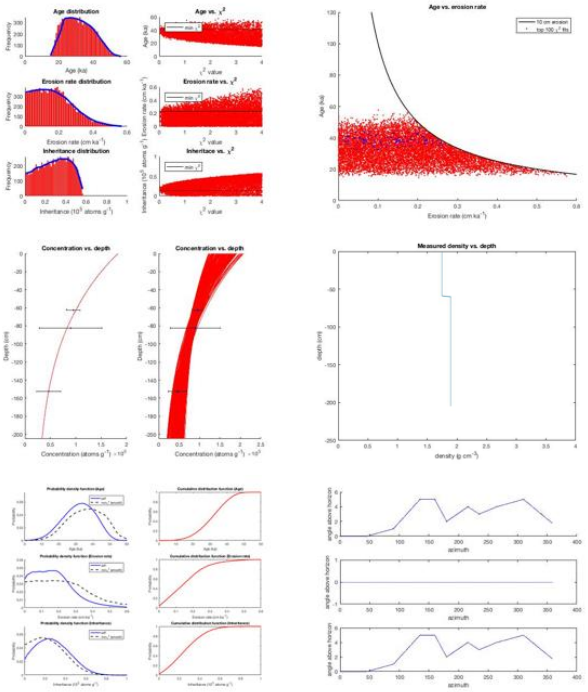

LTR-T5N (corrected for possible 25 cm soil inflation; uppermost sample not included in model; 2 sigma level; 10,000 runs)

	age (ka)	inheritance (10^4 atoms g^-1)	erosion rate (cm ka^-1)
mean	31.5	2.84	0.17
median	31.0	2.90	0.16
mode	26.5	2.88	0.16
min chi^2	41.3	1.06	0.17
maximum	58.5	5.80	0.60
minimum	14.4	0.00	0.00
Bayesian most probable	**33.9**	**2.39**	**0.18**
Bayesian 2-sigma upper	47.6	6.16	0.45
Bayesian 2-sigma lower	12.8	0.11	0.00

LTR-T5N: Be10 depth profile dating of surface LTR-T5N - All depth intervals included in model.

Model parameters and age results using Depth Profile Simulator from Hidy et al. (2000).

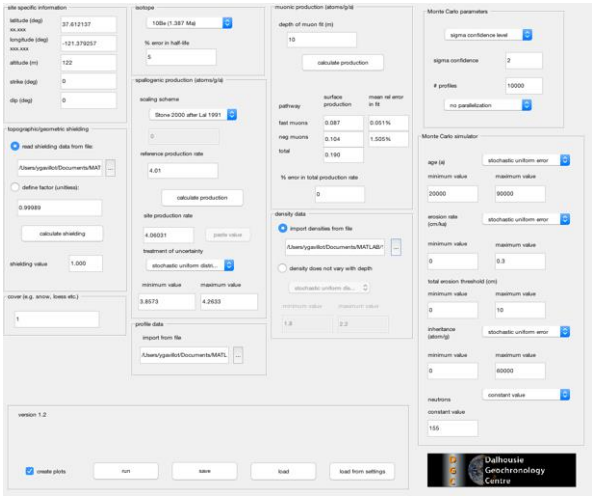

LTR-T5N model plots - All depth intervals included in model.

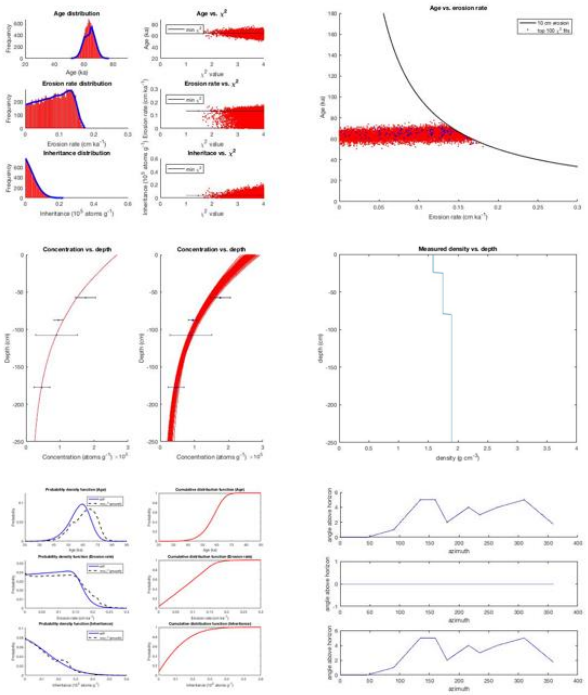

LTR-T5N (all samples included in model; 2 sigma level; 10,000 runs)

	age (ka)	inheritance (10^4 atoms g^-1)	erosion rate (cm ka^-1)
mean	63.6	0.42	0.08
median	63.6	0.33	0.09
mode	63.1	0.04	0.13
min chi^2	65.1	0.34	0.13
maximum	77.6	2.24	0.18
minimum	50.3	0.00	0.00
Bayesian most probable	**60.0**	**0.00**	**0.14**
Bayesian 2-sigma upper	69.0	3.54	0.19
Bayesian 2-sigma lower	40.1	NaN	NaN